ANL-ARC-204

# Final Report on Improved Creep-Fatigue Models on Advanced Materials for SFR Applications

**Nuclear Engineering Division**

**About Argonne National Laboratory**
Argonne is a U.S. Department of Energy laboratory managed by UChicago Argonne, LLC under contract DE-AC02-06CH11357. The Laboratory's main facility is outside Chicago, at 9700 South Cass Avenue, Argonne, Illinois 60439. For information about Argonne, see www.anl.gov.

**Availability of This Report**
This report is available, at no cost, at http://www.osti.gov/bridge. It is also available on paper to the U.S. Department of Energy and its contractors, for a processing fee, from:

U.S. Department of Energy
Office of Scientific and Technical Information
P.O. Box 62
Oak Ridge, TN 37831-0062
phone (865) 576-8401
fax (865) 576-5728
reports@adonis.osti.gov

**Disclaimer**
This report was prepared as an account of work sponsored by an agency of the United States Government. Neither the United States Government nor any agency thereof, nor UChicago Argonne, LLC, nor any of their employees or officers, makes any warranty, express or implied, or assumes any legal liability or responsibility for the accuracy, completeness, or usefulness of any information, apparatus, product, or process disclosed, or represents that its use would not infringe privately owned rights. Reference herein to any specific commercial product, process, or service by trade name, trademark, manufacturer, or otherwise, does not necessarily constitute or imply its endorsement, recommendation, or favoring by the United States Government or any agency thereof. The views and opinions of document authors expressed herein do not necessarily state or reflect those of the United States Government or any agency thereof, Argonne National Laboratory, or UChicago Argonne, LLC.

ANL-ARC-204

# Final Report on Improved Creep-Fatigue Models on Advanced Materials for SFR Applications

**Meimei Li, William K. Soppet, Saurin Majumdar, David Rink, and Ken Natesan**
Nuclear Engineering Division
Argonne National Laboratory

September 2011

# ABSTRACT

This report provides an update on the materials performance criteria and methodology relevant to sodium-cooled fast reactors (SFRs). The report is the second deliverable (Level 2) in FY11 (M2A11AN040303) under the work package A-11AN040303 "**Materials Performance Criteria and Methodology**" as part of the Advanced Structural Materials Program for the Advanced Reactor Concepts.

The overall objective of the Materials Performance Criteria and Methodology work project is to evaluate the key requirements for the ASME Code qualification and the Nuclear Regulatory Commission (NRC) approval of advanced structural materials in support of the design and performance of sodium-cooled fast reactors. Advanced materials are a critical element in the development of fast reactor technologies. Enhanced materials performance not only improves safety margins and provides design flexibility, but also is essential for the economics of future advanced fast reactors. Qualification and licensing of advanced materials are prominent needs for the development and implementation of advanced fast reactor technologies. Nuclear structural component designs in the U.S. comply with the ASME Boiler and Pressure Vessel (B&PV) Code Section III (Rules for Construction of Nuclear Facility Components), and the NRC grants licensing. As the SFRs will operate at higher temperatures than the current light water reactors (LWRs), the design of elevated-temperature components must comply with ASME Section III Subsection NH (Class 1 Components in Elevated Temperature Service). A number of technical issues relevant to materials performance criteria and high temperature design methodology in the SFR were identified and presented in earlier reports. A viable approach to resolve these issues and the R&D priority were also recommended. The development of mechanistically based creep-fatigue interaction models for life prediction and reliable data extrapolation was chosen to be the central focus in near-term efforts.

Our current focus is on the creep-fatigue damage issue in high-strength ferritic/martensitic steels such as mod.9Cr-1Mo (G91) and NF616 (G92) steels. The current ASME creep-fatigue design rule puts severe limits of fatigue and creep loads for G91 steel, the lead structural material for fast reactors. High-strength ferritic/martensitic steels behave fundamentally differently from austenitic stainless steels, for which the current ASME creep-fatigue design rules were developed. The unique deformation and damage characteristics in G91 steel, e.g. cyclic softening, degradation of creep and rupture strength during cyclic service, demands a new creep-fatigue design procedure that explicitly accounts for the material's unique creep-fatigue behavior. G92 steel, a variant of G91 steel, is the lead candidate in the Advanced Alloy Development program. There is currently no creep-fatigue design rule available for this advanced alloy.

To support the predictive model development and resolve the over-conservative issue with the ASME design rule for G91 steel, we recovered stress relaxation data from thirteen creep-fatigue tests conducted in the late 1980s and early 1990s at Oak Ridge National Laboratory, and conducted extensive data analysis in FY10. Based on this database and available literature data, we have developed a Cyclic Softening Model and a Stress Relaxation Model specifically applied to G91 steel. The Cyclic Softening Model describes the cyclic stress variation as a function of cycle number during creep-fatigue loading, and well captures the cyclic softening effect in G91 steel. The Stress Relaxation Model predicts the stress relaxation curve during the hold time of cyclic loading, and its dependence on the cyclic softening effect of G91 steel.

Two creep-fatigue test systems have been set up to conduct model-oriented creep-fatigue experiments. Results from three creep-fatigue experiments on Heat 30176 of G91 steel are presented in the report: (1) a test performed at 550°C with total strain amplitude of 0.25% and a hold time of 60 s applied at peak strains in both tension and compression, (2) a test performed at 400°C with total strain amplitude of 0.5% and a tension and compression hold time of 60 s, and (3) a test performed at 20°C with total strain amplitude of 0.5% and a tension and compression hold time of 60 s. Three different test temperatures were chosen for two primary reasons: to determine the transition temperature of creep-fatigue interaction from a plasticity-dominated process to a creep-dominated process; to develop unified creep-fatigue models applicable for a wide range of temperatures. With the detailed information obtained in the creep-fatigue experiments, we have further refined the Cyclic Softening Model and Stress Relaxation Model.

The Cyclic Softening Model and Stress Relaxation Model were incorporated into the Bilinear Creep-Fatigue Damage Model, forming a powerful framework for the life prediction by an improved creep-fatigue evaluation methodology. The cyclic softening and consecutive stress relaxation responses in G91 steel can be considered for each cycle of the entire cyclic process in the model calculation. The creep-fatigue damage in G91 steel was evaluated using the improved Bilinear Creep-Fatigue Damage Model without any safety margins. It was found that due to the significant cyclic softening in G91 steel, the unit creep damage in each cycle decreased continuously with increasing number of cycles. This continuous change in creep damage with cycling has significant implication in the evaluation of the total creep-fatigue damage. The total creep damage can be one order of magnitude lower when the unit creep damage at half-life was used in the evaluation in comparison with the calculations using the unit creep damage at cycle 10. An important conclusion was that the accurate assessment of the creep-fatigue damage in G91 steel must consider the history of cycling. This analysis provides a more realistic assessment of creep-fatigue damage and identifies critical factors that must be considered in the development of future advanced models for high-strength ferritic/martensitic alloys.

An accelerated creep-fatigue testing methodology is proposed for the design of model-oriented experiments to guide and validate model developments. Future work will focus on creep-fatigue experiments of both G91 and G92 steels, and development of creep-fatigue models applicable to advanced ferritic/martensitic alloys. The Cyclic Softening Model and Stress Relaxation Model will be improved by incorporating microstructural parameters of dislocation density, subgrain structure, and second-phase particles. Collaborative modeling of combined Cyclic Softening Model, Stress Relaxation Model, and Interactive Damage Rate Model will be pursued for life prediction under creep-fatigue loading with extended hold time. Accelerated, well-controlled creep-fatigue tests will be conducted to provide high-quality experimental data to refine key material parameters and validate models.

# TABLE OF CONTENTS

ABSTRACT ........ i
TABLE OF CONTENTS ........ iii
LIST OF TABLES ........ iv
LIST OF FIGURES ........ v
1 Introduction ........ 1
2 ASME Creep-Fatigue Design Rule for G91 Steel and Current Development ........ 3
3 Creep-Fatigue Experiments ........ 5
  3.1 Experimental Procedure ........ 5
  3.2 Experimental Results ........ 8
    3.2.1 Creep-Fatigue Data ........ 8
    3.2.2 Microstructure ........ 13
4 Modeling Creep-Fatigue Interaction ........ 14
  4.1 Cyclic Softening Model ........ 14
  4.2 Stress Relaxation Model ........ 18
  4.3 Improved Bilinear Creep-Fatigue Damage Model ........ 22
  4.4 Interactive Damage Rate Model ........ 29
5 Accelerated Creep-Fatigue Testing Methodology ........ 31
6 Summary and Future Work ........ 33
References ........ 35

_Toc272832930

# LIST OF TABLES

Table 3-1. Chemical composition of G91 steel and the ASME specifications .......................... 6

## LIST OF FIGURES

Figure 2-1. Creep-fatigue interaction diagram for ASME NH approved materials ......................4

Figure 3-1. Geometry and dimensions of creep-fatigue specimens ............................................6

Figure 3-2. Fabrication drawing of creep-fatigue specimens .....................................................7

Figure 3-3. High temperature creep-fatigue test system.............................................................7

Figure 3-4. Hysteresis loop..........................................................................................................9

Figure 3-5. Hysteresis loops for cycles 1, 10, 100, and 1000 for the specimen tested at 550°C with total strain amplitude of 0.25%, and a tension and compression hold time of 60 s (TCH 60 s) .........................................................................9

Figure 3-6. Hysteresis loops for cycles 1, 10, 100, and 1000 for the specimen tested at 400°C with total strain amplitude of 0.5%, and a tension and compression hold time of 60 s (TCH 60 s) .........................................................................9

Figure 3-7. Hysteresis loops for cycles 1, 10, 100, and 1000 for the specimen tested at 20°C with total strain amplitude of 0.5%, and a tension and compression hold time of 60 s (TCH 60 s) .......................................................................10

Figure 3-8. Plastic strain amplitude as a function of cycles for G91 tested at 550°C with total strain amplitude of 0.25%, 400°C with total strain amplitude of 0.5% and 20°C with total strain amplitude of 0.5%, respectively. All three tests were carried out with a tension and compression hold time of 60 s in air .......................10

Figure 3-9. Cyclic stress as a function of cycles (a) in linear scale and (b) in log scale for the G91 specimens tested at 550°C with total strain amplitude of 0.25%, 400°C with total strain amplitude of 0.5% and 20°C with total strain amplitude of 0.5%, respectively. All three tests were carried out with a tension and compression hold time of 60 s (TCH 60 s) in air.............................................11

Figure 3-10. (a) Relaxed stress as a function of time during hold and (b) normalized relaxed stress as a function of time during hold for the G91 specimen tested at 550°C with total strain amplitude of 0.25%, and a hold time of 60 s applied at peak strains in tension and compression (TCH 60 s)..............................................12

Figure 3-11. (a) Relaxed stress as a function of time during hold and (b) normalized relaxed stress as a function of time during hold for the G91 specimen tested at 400°C with total strain amplitude of 0.5%, and a hold time of 60 s applied at peak strains in tension and compression (TCH 60 s)..............................................12

Figure 3-12. (a) Relaxed stress as a function of time during hold and (b) normalized relaxed stress as a function of time during hold for the G91 specimen tested at 20°C with total strain amplitude of 0.5%, and a hold time of 60 s applied at peak strains in tension and compression (TCH 60 s)..............................................13

Figure 3-13. Microstructure of the specimen tested at 550°C with total strain amplitude of 0.25%, and a tension and compression hold time of 60 s .......................................14

Figure 3-14. Microstructure of the specimen tested at 20°C with total strain amplitude of 0.5%, and a tension and compression hold time of 60 s ..........14

Figure 4-1. Cyclic hardening (a) constant strain control, (b) stress response, (c) cyclic stress-strain response ..........15

Figure 4-2. Cyclic softening (a) constant strain control, (b) stress response, (c) cyclic stress-strain response ..........15

Figure 4-3. Tensile curves of G91 tested at 20 and 550°C ..........16

Figure 4-4. Calculated cyclic softening curves for G91 steel for total strain ranges of 0.5–1.5% at 550°C ..........17

Figure 4-5. Comparison of the modeled cyclic softening curves with experimental data in (a) linear scale and (b) log scale, for G91 specimens tested at 550°C with total strain amplitude of 0.25%, 400°C with total strain amplitude of 0.5% and 20°C with total strain amplitude of 0.5%, respectively. All three tests were carried out with a hold time of 60 s applied at peak strains in tension and compression (TCH 60 s) in air ..........18

Figure 4-6. Stress relaxation during hold time ..........19

Figure 4-7. Comparison of modeled stress relaxation curves with experimental data for cycles 1, 10, 100, and 1000 for G91 tested at 20°C, 0.5% total strain amplitude with a tension and compression hold time of 60 s ..........21

Figure 4-8. Comparison of modeled stress relaxation curves with experimental data for cycles 1, 10, 100, and 1000 for G91 tested at 400°C, 0.5% total strain amplitude with a tension and compression hold time of 60 s ..........21

Figure 4-9. Comparison of modeled stress relaxation curves with experimental data for cycles 1, 10, 100, and 1000 for G91 tested at 550°C, 0.25% total strain amplitude with a tension and compression hold time of 60 s ..........22

Figure 4-10. Compilation of the fatigue data in terms of the total strain range and the cycle to failure under continuous cycling for five commercial heats of G91 steel tested at 538 and 593°C in air. Tests were performed at Oak Ridge National Laboratory. Data were taken from the literature. The solid line represents the average strain-life relation ..........23

Figure 4-11. Compilation of the creep rupture data in terms of the applied stress and the rupture life for five commercial heats of G91 steel tested at 538 and 593°C in air. Tests were performed at Oak Ridge National Laboratory. Data were taken from the literature. The solid lines represent the average creep rupture behavior......24

Figure 4-12. Unit creep damage as a function of the number of cycles for G91 steel tested in creep-fatigue conditions at 535°C (C60–compression hold for 60 min, T60–tension hold for 60 min, and TCH60–tension and compression hold for 60 min) ......25

Figure 4-13. Unit creep damage as a function of the number of cycles for G91 steel tested in creep-fatigue conditions at 593°C ..........25

Figure 4-14. An example showing the creep damage rate and the accumulation of creep damage as a function of hold time per unit cycle for G91 steel ..................................26

Figure 4-15. Creep-fatigue interaction diagram calculated using the unit creep damage at the half-life for G91 steel. The dash lines represent the ASME creep-fatigue damage envelope for G91 steel with the intersection of (0.01, 0.1) ............................27

Figure 4-16. Creep-fatigue interaction diagram calculated using the unit creep damage at cycle 10 for G91 steel. The dash lines represent the ASME creep-fatigue damage envelope for G91 steel with the intersection of (0.01, 0.1) ............................27

Figure 4-17. Creep-fatigue interaction diagram calculated by integration of unit creep damage vs. cycles curves for G91 steel. The dash lines represent the ASME creep-fatigue damage envelope for G91 steel with the intersection of (0.01, 0.1) ......28

Figure 5-1. Accelerated creep-fatigue damage testing methodology ...........................................32

# 1 Introduction

Economical competitiveness is a key element in the development of advanced reactor technologies. Advanced materials allow compact and simple design of sodium cooling systems and reactor structure, and have the potential to reduce construction- and operational-costs for advanced fast reactors. The Advanced Materials Program under Advanced Reactor Concepts is responsible for developing materials for improved economics, reliability, safety, and design flexibility for liquid metal reactors (LMR). High temperature-, corrosion- and irradiation-resistant alloys are being evaluated for the LMR design. The materials performance criteria and high temperature design methodology are critical elements in the development of advanced fast reactor technologies.

The construction of nuclear structural components in the U.S. must comply with the ASME Boiler and Pressure Vessel (B&PV) Code Section III – Rules for Construction of Nuclear Power Plant Components. Nuclear Regulatory Commission (NRC) grants the construction/operation license for the nuclear power plant. Since the sodium-cooled fast reactor (SFR) will have sodium outlet temperature of 500-550°C and a 60-yr design life, significantly different from the current light water reactors (LWRs), the design of elevated-temperature components in SFRs must comply with ASME Section III Subsection NH–Class 1 Components in Elevated Temperature Service. The design of SFA components must also consider time-dependent effects on mechanical properties such as creep, creep-fatigue, and creep ratcheting. The NRC licensing review of the Clinch River Breeder Reactor Plant (CRBRP) and the Power Reactor Innovative Small Module (PRISM) project identified a number of technical issues including creep-fatigue evaluation, weldment safety evaluation, notch weakening effect, etc. Many of these issues remain unresolved.

ASME Subsection NH provides the high temperature design rules for components in nuclear service. The rules were developed in support of the U.S. liquid metal fast breeder reactor (LMFBR) program in 1960s and 70s. Subsection NH has a rather limited choice of materials with only five materials qualified, which include Type 304 and 316 austenitic stainless steels, 2.25Cr-1Mo steel, modified 9Cr-1Mo (G91) steel, and Alloy 800H. Adequate database must be established for any new materials to be included in Subsection NH, if they are used in the high-temperature reactor design. In addition to generating data for qualifying the advanced materials, high temperature design rules must also be developed to account for high temperature damages such as excessive creep deformation, creep rupture, cyclic creep ratcheting, creep-fatigue, and also consider environmental effects of corrosion and neutron irradiation on these properties. A detailed in-depth assessment of materials' qualification and licensing needs was conducted and the findings were reported [Natesan et al. 2008]. A list of key technical issues was identified and a viable approach to resolve these issues and the R&D priority were recommended [Natesan et al. 2009]. Among them, creep-fatigue damage was identified as the most critical issue in high temperature structural designs.

It is recognized that the current creep-fatigue design rule adopted in the ASME Code is empirical and relies heavily on a large amount of laboratory data. It allows no reliable extrapolation to real reactor environments with adequate fidelity. The creep-fatigue life predictive models, based on a solid fundamental understanding of damage mechanism, are essential for new reactor designs where operating temperatures are higher and the design life sufficiently longer than current experience. With the near-term goal of developing physically-sound predictive models for creep-fatigue damage in advanced structural alloys and ultimately developing a robust design methodology, our current effort focuses on developing a validated creep-fatigue predictive model for high-strength ferritic/martensitic steels, e.g. G91 and G92 steels. G91 steel is an ASME Code qualified material. It currently faces severe limitations of design loads due largely to the over-conservatism of the ASME creep-fatigue design rule. G92 is a variant of G91 steel with significantly improved high temperature properties, and is being developed for use in next-generation fast reactors. G92 steel is, currently, not included ASME NH, and no creep-fatigue design rule is available in ASME Code.

Creep-fatigue interaction is a complex dynamic process involving combined effects of creep and fatigue (and environmental effects) on the accumulated damage. The process depends on a large number of mechanical and metallurgical factors including test temperature, strain rate, hold time, types of hold, environment, thermo-mechanical treatment, microstructure, etc. The mechanisms of creep-fatigue damage are not well understood, and consequently, predictive capabilities are limited.

High-strength ferritic-martensitic steels have unique deformation characteristics that are significantly different from those of austenitic stainless steels and low alloy steels under creep-fatigue conditions. G91 is subjected to considerable cyclic softening during strain-controlled cyclic loading [Kim and Weertman 1988, Kannan et al. 2009, Shankar et al. 2006]. The stress amplitude decreases as the number of cycle increases. This is in contrast with austenitic stainless steel, Type 304 and 316, which cyclically harden [Marshall 1984]. The cyclic behavior of G91 steel is also different from that of annealed 2.25Cr-1Mo steel, in that annealed 2.25Cr-1Mo experiences cyclic hardening, cyclic softening, or a mixture of cyclic hardening and softening, depending on temperature, strain rate, and hold time [Jaske et al. 1975]. Cyclic softening in G91 occurs at all temperatures between 25 and 600°C in both continuous fatigue and creep-fatigue tests [Kim and Weertman 1988]. The initial high strength advantage of the alloy is lost even after a small number of loading cycles. Depending on the strain range and strain rate, this stress may drop to nearly one-half of its starting value [Matsuoka et al. 1984].

To evaluate the creep damage under creep-fatigue loading conditions, it is necessary to have a good knowledge of stress variation during the hold time. When a hold time is applied at peak strains either in tension or in compression or under a combination of tension and compression, stress relaxes with time due to conversion of the elastic strain into the inelastic strain when the total strain is kept constant. Stress relaxation data during the hold time is critical in evaluating materials inelastic behavior and deformation characteristics and estimating creep damage under creep-fatigue conditions.

In this report, we have presented Cyclic Softening Model and Stress Relaxation Model that were recently developed specifically for G91 steel. These models were incorporated into the Bilinear Creep-Fatigue Model to form a powerful framework for the prediction of the lifetime under creep-fatigue loading. Results from three creep-fatigue experiments are also presented that were conducted to improve and validate creep-fatigue models. The report also discusses future work in extending the Cyclic Softening Model and Stress Relaxation Model to the Interactive Damage Rate Equations and designing and conducting model-oriented, accelerated creep-fatigue experiments to aid in model development and validation for G91 and G92 steels.

## 2 ASME Creep-Fatigue Design Rule for G91 Steel and Current Development

Creep-fatigue damage is one of the most severe structural failure modes in elevated temperature design. In ASME Section III Subsection NH, creep-fatigue life is evaluated with a linear summation of fractions of cyclic damage and creep damage. The creep-fatigue criterion is given by:

$$\underbrace{\sum_j \left(\frac{n}{N_d}\right)_j}_{\text{Cyclic Damage}} + \underbrace{\sum_k \left(\frac{\Delta t}{T_d}\right)_k}_{\text{Creep Damage}} \leq D \tag{2-1}$$

where $n$ and $N_d$ are the number of cycles of type $j$ and allowable number of cycles of the same cycle type, respectively; and $\Delta t$ and $T_d$ are actual time at stress level $k$ and allowable time at that stress level, respectively; $D$ is allowable combined damage fraction. Since the creep damage term is evaluated as a ratio of actual time versus allowable time, it is generally referred to as time-fraction.

The cyclic- and creep-damage terms on the left hand side of Eq. (2-1) are evaluated in an uncoupled manner. The interaction of creep and fatigue is accounted for empirically by the $D$ term on the right side of the equation. This can be represented graphically by the creep-fatigue interaction diagram, which is shown schematically for the NH materials in Fig. 2-1 [ASME 2011]. The NH creep-fatigue interaction curves were established empirically through data correlation. Such an engineering approach often proves to be effective when it is supported by a robust database that is representative of the operating conditions and when it does not involve significant data extrapolation. A multi-pronged approach is employed in NH in order to ascertain that the design life determined from the creep-fatigue criterion is adequately conservative.

With the extended design life of 60 years or longer for non-replaceable components in advanced reactors, it is critical that the models used to calculate design lives are accurate and reliable. This is more so for the creep-fatigue life, because the current life prediction methods are based empirically on laboratory test data that are necessarily short-term (typically a few thousand hours) in duration relative to the reactor life. Thus, design life prediction requires significant extrapolation beyond the database from which the empirical constants are derived for the predictive methods. The reliability of the life-prediction methods would be greatly enhanced, if they were based on an understanding of the mechanisms underlying the damage processes.

It has been recognized that the creep-fatigue design procedure for G91 steel is overly conservative [Asayama and Tachibana 2007, Asayama 2006, 2010, Riou 2007]. As shown in Fig. 2-1, the creep-fatigue damage envelope for G91 has the interception point of (0.1, 0.01), which results in conservative creep-fatigue design, especially for the creep load. The modification of the interception point from (0.1, 0.01) to (0.3, 0.3) is being suggested to allow more reasonable life prediction [Asayama et al. 2010]. While this recommendation may provide an intermediate solution, the complex creep-fatigue problem associated with G91 steel due to its unique degradation mechanisms calls for an advanced creep-fatigue design procedure that explicitly accounts for the material's unique deformation and failure behavior.

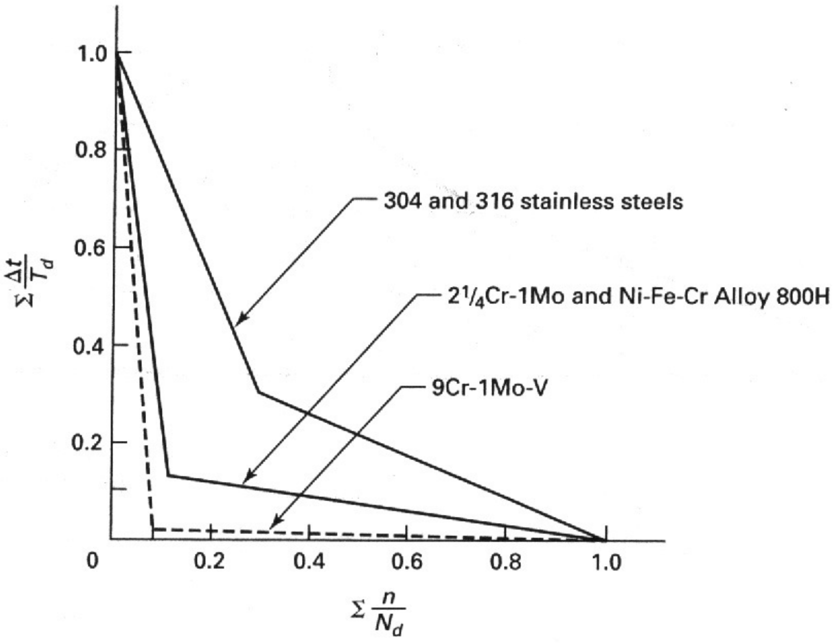

Figure 2-1. Creep-fatigue interaction diagram for ASME NH approved materials.

# 3 Creep-Fatigue Experiments

## 3.1 Experimental Procedure

Creep-fatigue specimens were fabricated from heat 30176 of G91 steel. The material was provided in the form of 1-in. thick plate by Oak Ridge National Laboratory. The chemical compositions of the alloy are given in Table 3-1 [DiStefano et al. 1986]. The specifications of ASTM SA-387 are also included in Table 3-1 for comparison. It is noted that the content of silicon in heat 30176 is below the ASTM specification. The alloy was normalized at 1050°C for 1 h, air cooled, tempered at 760°C for 2 h, and air cooled.

ASTM standard-size round specimens were used in the creep-fatigue tests (ASTM E8 – Standard Test Methods for Tension Testing of Metallic Materials). The geometry and dimensions of the creep-fatigue specimens are shown in Fig. 3-1. The specimens have a gauge diameter of 0.156 in, gauge length of 0.5 in, and total length of 4.5 in. The gauge length is along the rolling direction, as shown in Fig. 3-2. Gauge sections of the creep-fatigue specimens were polished longitudinally with 1-μm diamond paste to remove surface scratches and oxide layer, if any, before testing.

Creep-fatigue tests were performed on an MTS closed-loop servo-hydraulic test frame. Specimen heating was provided by a three-zone split furnace. The test temperature was controlled and monitored by two Type K thermocouples wired at the top and bottom grip sections of the specimen. All the creep-fatigue tests were carried out in air. The tests were performed under constant total strain amplitude in fully reversed (R = -1) strain control. A high temperature furnace extensometer was used to measure the total axial strain. The setup of creep-fatigue experiments is shown in Fig. 3-3.

Hold-time creep-fatigue tests were performed with a trapezoidal waveform with the hold time applied at peak strains. The strain rates in tension and compression were kept the same, 0.001 $s^{-1}$ for all the tests. Tests were carried out under computer control using the Instron WaveMatrix$^{TM}$ Dynamic and Fatigue Materials Testing Software. The stress-strain hysteresis loop and maximum and minimum stresses of a cycle were recorded at intervals throughout the test.

Microstructure of the creep-fatigued specimen was examined by transmission electron microscopy. TEM discs of 3-mm in size were made from the gauge section of the specimen after the creep-fatigue test.

Table 3-1. Chemical composition of G91 steel and the ASME specifications.

| | 30176 Plate | G91 (SA-387/SA-387M) |
|---|---|---|
| C | 0.081 | .06-.15 |
| Mn | 0.37 | .25-.66 |
| P | 0.01 | .025(max) |
| S | 0.003 | .012(max) |
| Si | 0.11 | .18-.56 |
| Ni | 0.09 | .43(max) |
| Cr | 8.61 | 7.9-9.6 |
| Mo | 0.89 | .8-1.1 |
| V | 0.209 | .16-.27 |
| Nb | 0.072 | .05-.11 |
| Ti | 0.004 | .01(max) |
| Co | 0.01 | |
| Cu | 0.04 | |
| Al | 0.007 | .02(max) |
| B | <.09 | |
| W | <.01 | |
| As | 0.001 | |
| Sn | <.001 | |
| Zr | <.002 | .01(max) |
| N | 0.055 | .025-.08 |

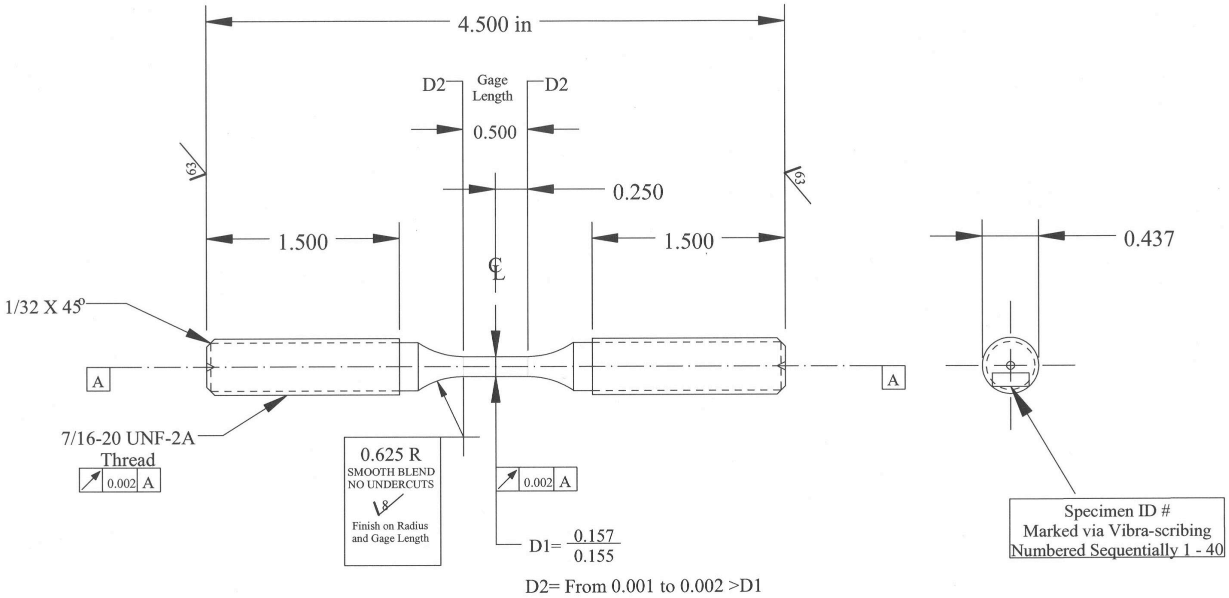
4.500 in
D2
Gage Length
D2
0.500
0.250
63
63
1.500
1.500
0.437
℄
1/32 X 45°
A
A
7/16-20 UNF-2A Thread
0.002 A
0.625 R
SMOOTH BLEND
NO UNDERCUTS
8
Finish on Radius and Gage Length
0.002 A
D1= 0.157 / 0.155
D2= From 0.001 to 0.002 >D1
Specimen ID #
Marked via Vibra-scribing
Numbered Sequentially 1 - 40

Figure 3-1. Geometry and dimensions of creep-fatigue specimens.

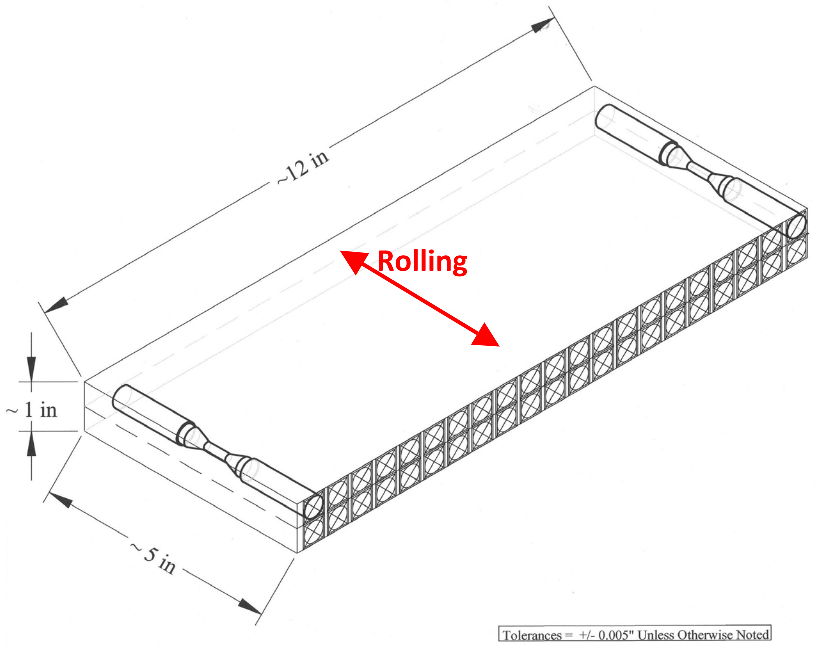
~12 in
Rolling
~ 1 in
~ 5 in
Tolerances = +/- 0.005" Unless Otherwise Noted

Figure 3-2. Fabrication drawing of creep-fatigue specimens.

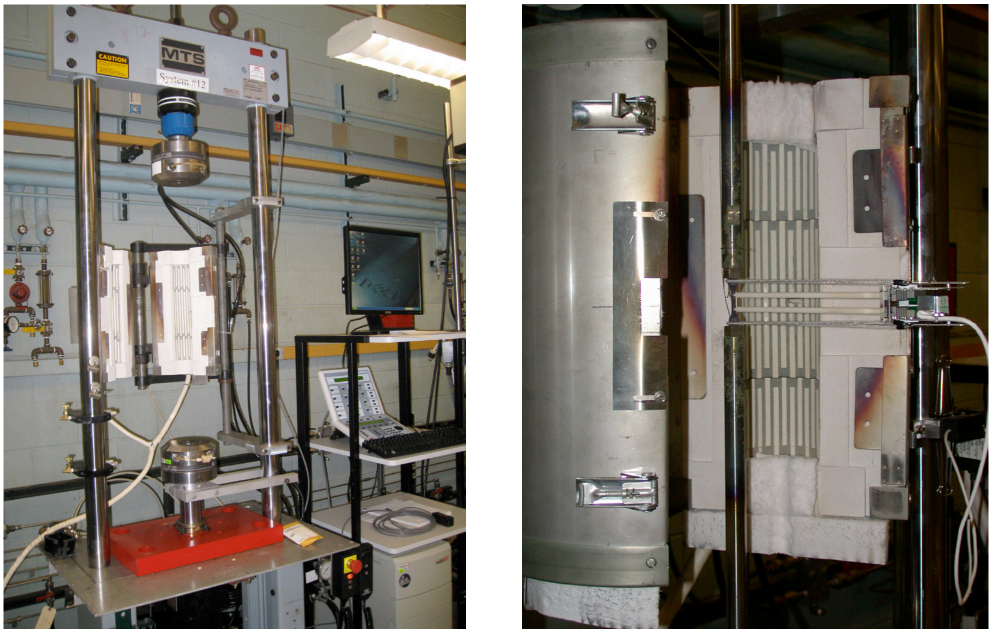
MTS
System #12

Figure 3-3. High temperature creep-fatigue test system.

## *3.2 Experimental Results*

### *3.2.1 Creep-Fatigue Data*

Data of three creep-fatigue tests are reported here: (1) a test performed at 550°C with total strain amplitude of 0.25% and a hold time of 60 s applied at peak strains in both tension and compression, (2) a test performed at 400°C with total strain amplitude of 0.5% and a hold time of 60 s applied at peak strains in both tension and compression, and (3) a test performed at 20°C with total strain amplitude of 0.5% and a hold time of 60 s applied at peak strains in both tension and compression. All three tests were carried out in air. Three different test temperatures were chosen for two primary reasons: to determine the transition temperature of creep-fatigue interaction from a plasticity-dominated process to a creep-dominated process; to develop unified creep-fatigue models applicable for a wide range of temperatures.

Hysteresis Loops

The response of a material under cyclic loading can be represented by a stabilized hysteresis loop, shown in Fig. 3-4 [Bannantine et al 1990]. The total width of the loop is the total strain range, $\Delta\varepsilon_t$. The total height of the loop is the total stress range, $\Delta\sigma$. The area inside the loop is the total energy dissipated during one cycle that represents the plastic deformation work done on the material. A total strain range, $\Delta\varepsilon_t$ is the sum of a plastic strain range, $\Delta\varepsilon_p$, and an elastic strain range, $\Delta\varepsilon_e$, i.e.

$$\Delta\varepsilon_t = \Delta\varepsilon_e + \Delta\varepsilon_p \tag{3-1}$$

The hysteresis loops for cycles 1, 10, 100 and 1000 for the specimen tested at 550°C with total strain amplitude of 0.25%, and a tension and compression hold time of 60 s are shown in Fig. 3-5. The loops widened continuously as the number of cycles increased; the stress range (or amplitude) continued to drop, indicating a significant cyclic softening effect. Stress relaxation is evident throughout the cyclic process. The hysteresis loops for cycles 1, 10, 100 and 1000 for the specimens tested at 400°C and 20°C are shown in Figs. 3-6 and 3-7, respectively.

The values of plastic strain amplitudes were measured from the maximum width of the hysteresis loops, and plotted as a function of cycles (solid lines) in Fig. 3-8. The plastic strain amplitude increased monotonically with the increase of the number of cycles. The evolution of the plastic strain followed a power law, and can be described by the following equations (shown in dash lines):

$$\begin{aligned} \Delta\varepsilon_p/2 &= 0.216\cdot(N)^{0.042} \quad (20^\circ C) \\ \Delta\varepsilon_p/2 &= 0.269\cdot(N)^{0.028} \quad (400^\circ C) \\ \Delta\varepsilon_p/2 &= 0.086\cdot(N)^{0.071} \quad (550^\circ C) \end{aligned} \tag{3-2}$$

The power exponent for the 550°C test is noticeably higher than those for the 20 and 400°C tests.

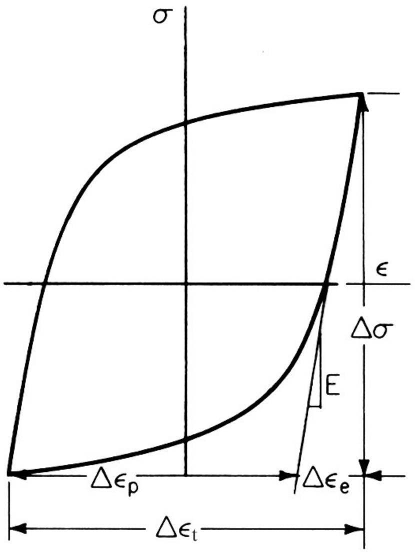

Figure 3-4. Hysteresis loop.

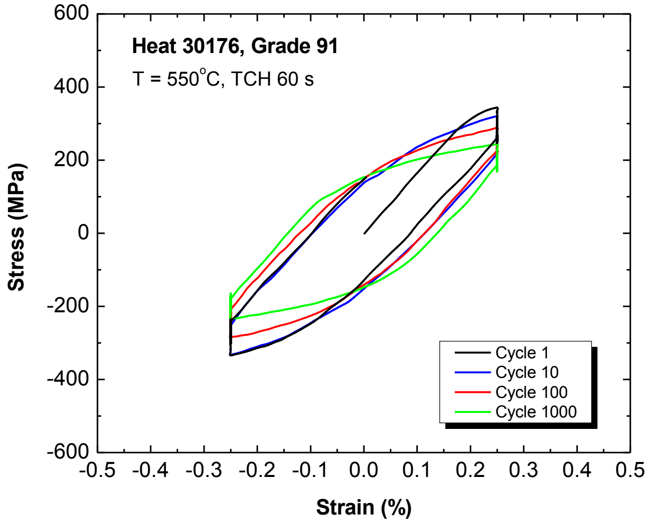

Figure 3-5. Hysteresis loops for cycles 1, 10, 100, and 1000 for the specimen tested at 550°C with total strain amplitude of 0.25%, and a tension and compression hold time of 60 s (TCH 60 s).

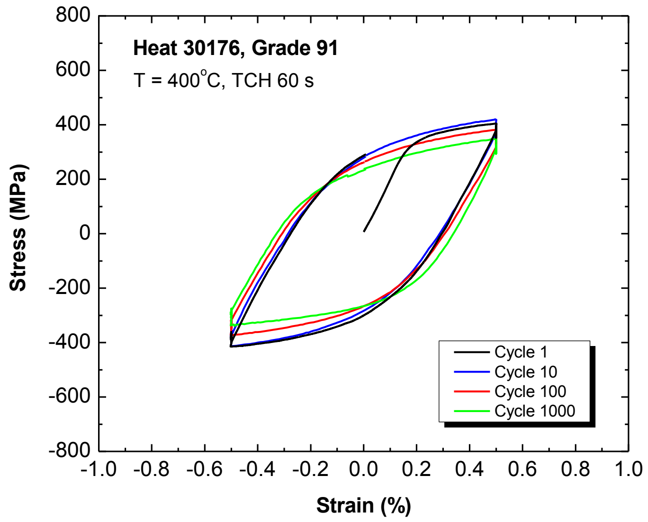

Figure 3-6. Hysteresis loops for cycles 1, 10, 100, and 1000 for the specimen tested at 400°C with total strain amplitude of 0.5%, and a tension and compression hold time of 60 s (TCH 60 s).

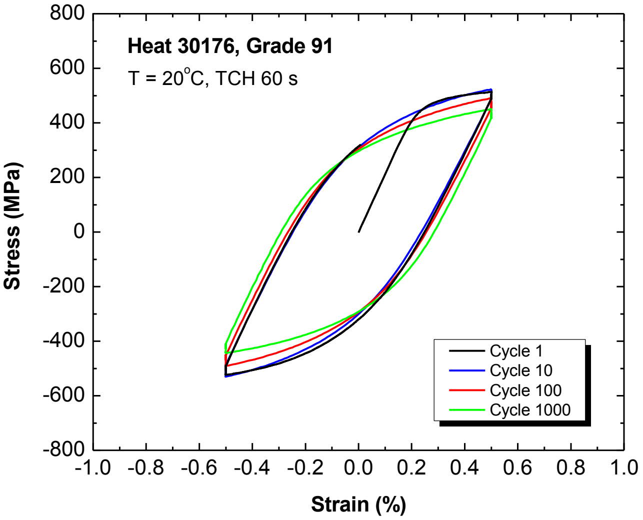

Figure 3-7. Hysteresis loops for cycles 1, 10, 100, and 1000 for the specimen tested at 20°C with total strain amplitude of 0.5%, and a tension and compression hold time of 60 s (TCH 60 s).

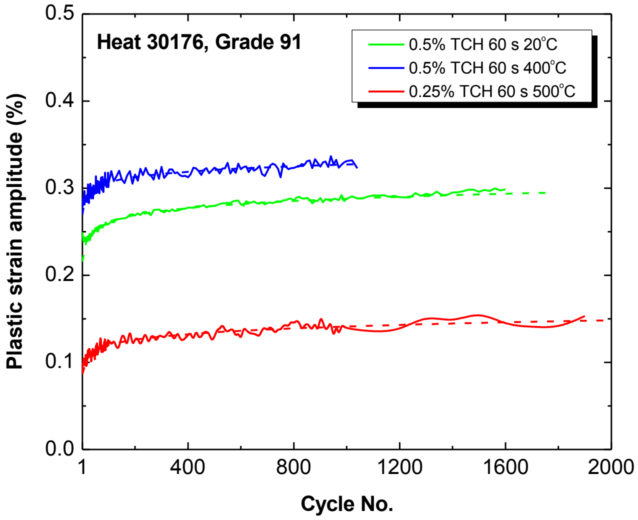

Figure 3-8. Plastic strain amplitude as a function of cycles for G91 tested at 550°C with total strain amplitude of 0.25%, 400°C with total strain amplitude of 0.5% and 20°C with total strain amplitude of 0.5%, respectively. All three tests were carried out with a tension and compression hold time of 60 s in air.

.

## Cyclic Behavior

The peak stresses in tension and compression are plotted as a function of the number of cycles in Fig. 3-9 (a) in linear scale and (b) in log scale for the specimens tested at 550°C with total strain amplitude of 0.25%, 400°C with total strain amplitude of 0.5%, and 20°C with total strain amplitude of 0.5%, with a tension and compression hold of 60 s. A common characteristic of the stress response is that the stress continues to decrease with increasing cycles after the initial transient stage (up to ~10 cycles) at all three temperatures, so-called cyclic softening. In the transient stage, the alloy showed a slight cyclic hardening at 20 and 400°C, and a cyclic softening at 550°C. No saturation of the cyclic stress was observed in any of these test conditions. The profiles of cyclic stress response with cycle number are similar in tension and compression.

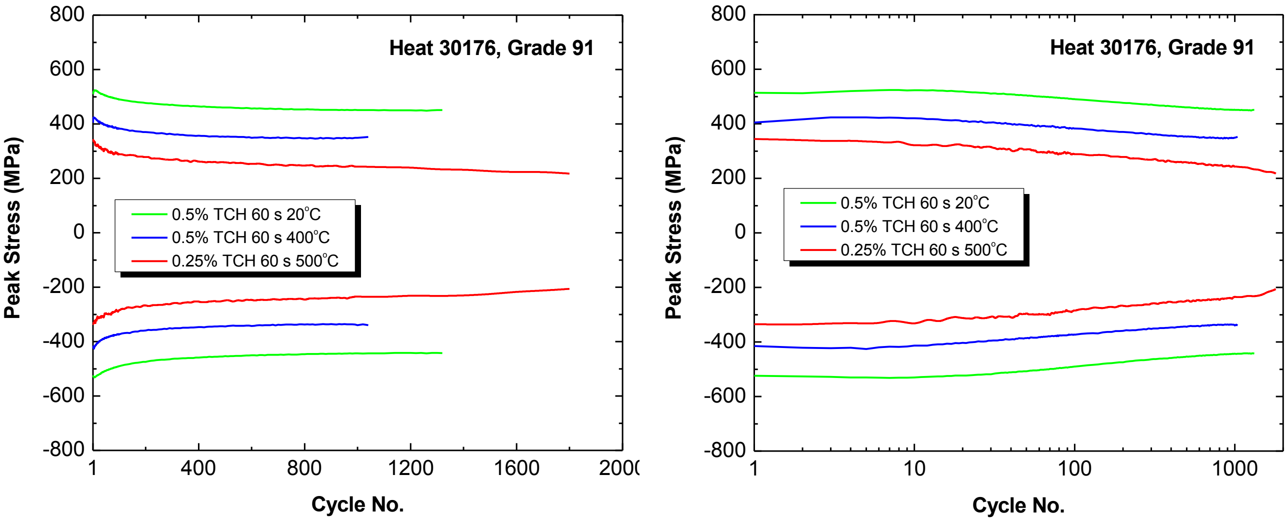

(a) (b)

Figure 3-9. Cyclic stress as a function of cycles (a) in linear scale and (b) in log scale for the G91 specimens tested at 550°C with total strain amplitude of 0.25%, 400°C with total strain amplitude of 0.5% and 20°C with total strain amplitude of 0.5%, respectively. All three tests were carried out with a tension and compression hold time of 60 s (TCH 60 s) in air.

## Stress Relaxation during Hold Time

Due to the fixed total strain level during the hold time in the creep-fatigue tests, stress relaxation was always observed at peak strains. There is an apparent stress drop from the peak stress in both tension and compression. Figure 3-10(a) shows the stress relaxation profiles during both tension and compression hold for cycles 1, 10, 100 and 1000 for the specimen tested at 550°C with total strain amplitude of 0.25% and a tension and compression hold of 60 s. The normalized stress relaxation curves are shown in Fig. 3-10(b). The stress relaxation curves for the tests conducted at 400 and 20°C with total strain amplitude of 0.5% and a tension and compression hold time of 60 s are shown in Figs. 3-11 and 3-12, respectively. The stress relaxation profiles are similar in shape and magnitude for the tension and compression parts of the cycling for all three tests. The normalized stress relaxation curves showed little dependence on the number of cycles.

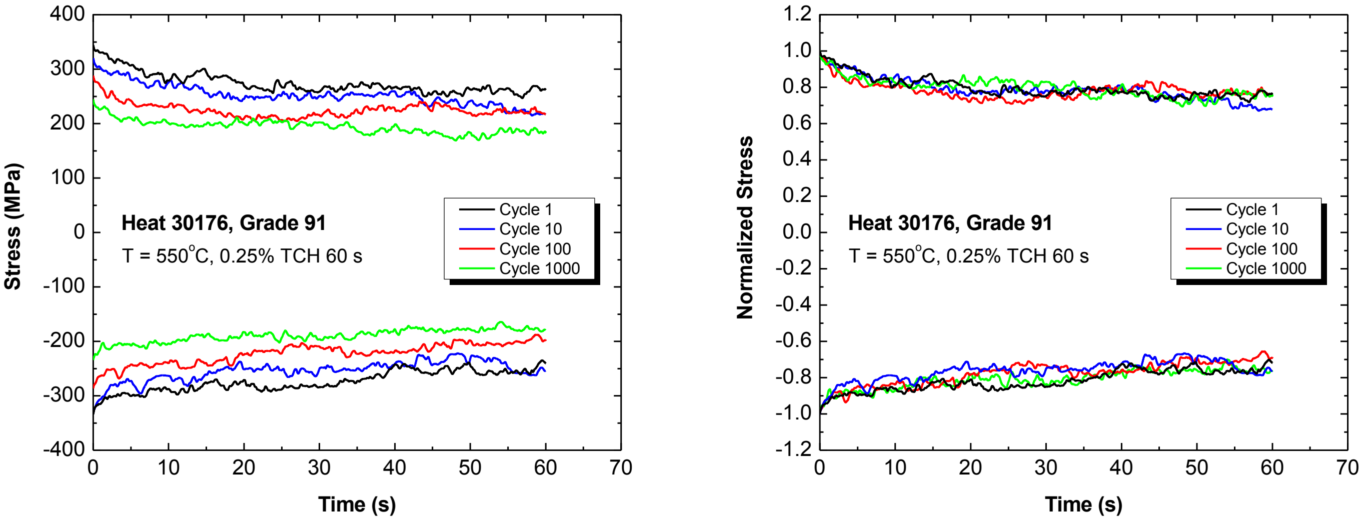

(a) (b)

Figure 3-10. (a) Relaxed stress as a function of time during hold and (b) normalized relaxed stress as a function of time during hold for the G91 specimen tested at 550°C with total strain amplitude of 0.25%, and a hold time of 60 s applied at peak strains in tension and compression (TCH 60 s).

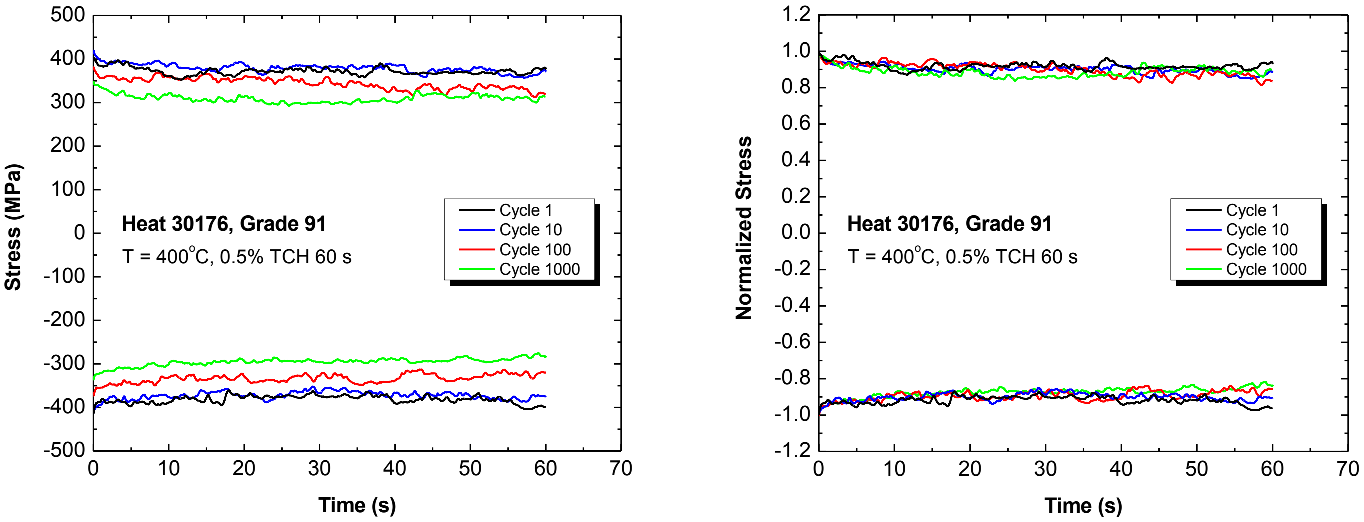

(a) (b)

Figure 3-11. (a) Relaxed stress as a function of time during hold and (b) normalized relaxed stress as a function of time during hold for the G91 specimen tested at 400°C with total strain amplitude of 0.5%, and a hold time of 60 s applied at peak strains in tension and compression (TCH 60 s).

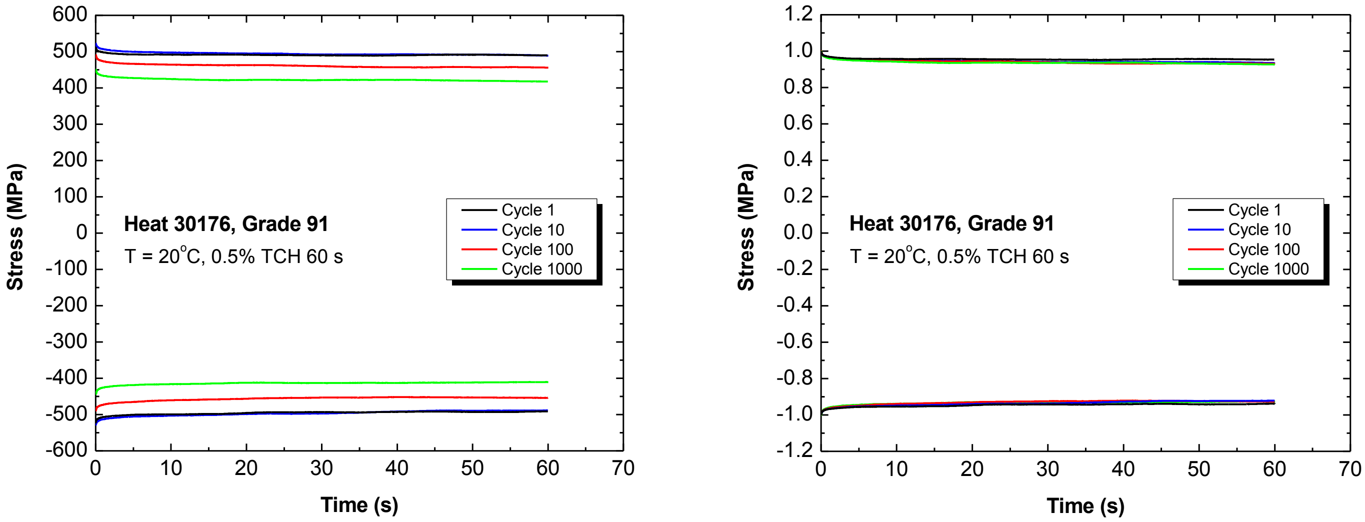

(a) (b)

Figure 3-12. (a) Relaxed stress as a function of time during hold and (b) normalized relaxed stress as a function of time during hold for the G91 specimen tested at 20°C with total strain amplitude of 0.5%, and a hold time of 60 s applied at peak strains in tension and compression (TCH 60 s).

### *3.2.2 Microstructure*

Microstructures are shown in Fig. 3-13 for the creep-fatigue specimen tested at 550°C with total strain amplitude of 0.25% and a tension and compression hold time of 60 s and in Fig. 3-14 for the specimen tested at 20°C with total strain amplitude of 0.5% and a tension and compression hold time of 60 s, respectively. The microstructure of the normalized and tempered G91 steel consists of martensite lath structure, high density of dislocations, and $M_{23}C_6$ carbides, and MX carbonitrides. This microstructure is stable during 550°C thermal exposure as found in our thermal aging study. However when tested under creep-fatigue loading, the microstructure experienced dramatic changes as shown in Figs. 3-13 and 3-14. The martensite lath structure evolved into well-organized, fine subgrain structure with a significantly lower density of dislocations within subgrains. The subgrain size in the 20°C test is smaller than that in the 550°C test, primarily due to the higher total strain amplitude (0.5%) in the 20°C test than that in the 550°C test (0.25%) [Kim and Weertman 1988].

TEM observations revealed that dislocation movement and rearrangement is the main cyclic deformation mechanism under the tested conditions. The formation of cell and subgrain structure in the creep-fatigued specimens correlates well with the observed cyclic softening behavior of G91 steel.

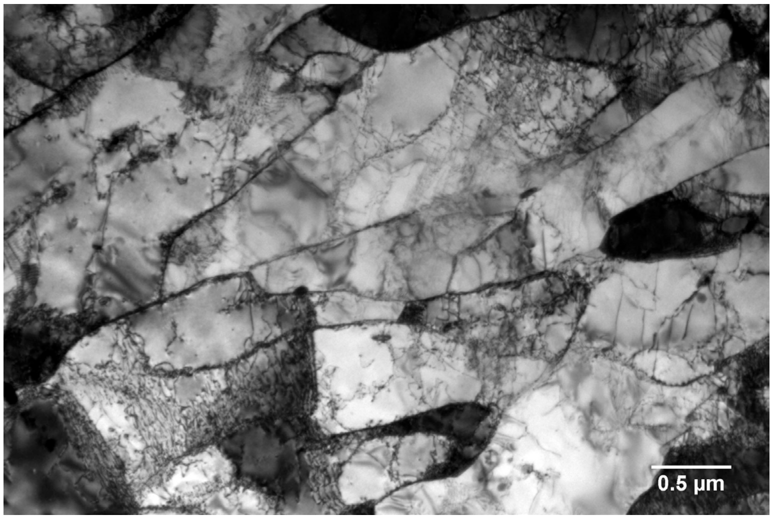

Figure 3-13. Microstructure of the specimen tested at 550°C with total strain amplitude of 0.25%, and a tension and compression hold time of 60 s.

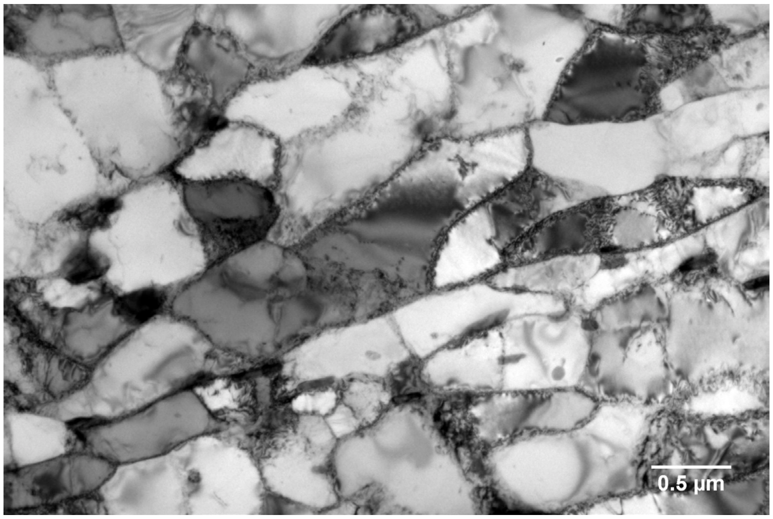

Figure 3-14. Microstructure of the specimen tested at 20°C with total strain amplitude of 0.5%, and a tension and compression hold time of 60 s.

# 4 Modeling Creep-Fatigue Interaction

## *4.1 Cyclic Softening Model*

One of the key issues in evaluating creep-fatigue damage in G91 steel is its continuous degradation of tensile and creep properties during cyclic service. The cyclic softening behavior of G91 steel must be properly understood and incorporated into the creep-fatigue evaluation procedure.

At the early stage of cyclic loading in constant strain control mode, the stress range of each cycle can be different. Depending on its initial condition, the material may be cyclically hardened or cyclically softened. As shown in Fig. 4-1 [Bannantine et al 1990], for an initially soft material, the stress range may increase with increasing cycle number. This is called cyclic hardening. Alternately, for an initially hard material, the stress range may decrease with each cycle of strain, and this is called cyclic softening (shown in Fig. 4-2 [Bannantine et al 1990]).

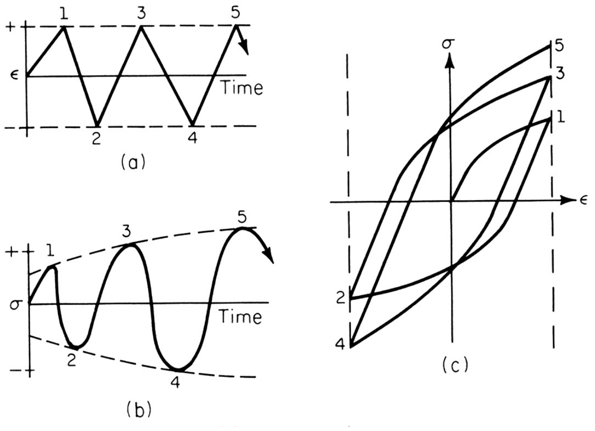

Figure 4-1. Cyclic hardening (a) constant strain control, (b) stress response, (c) cyclic stress-strain response.

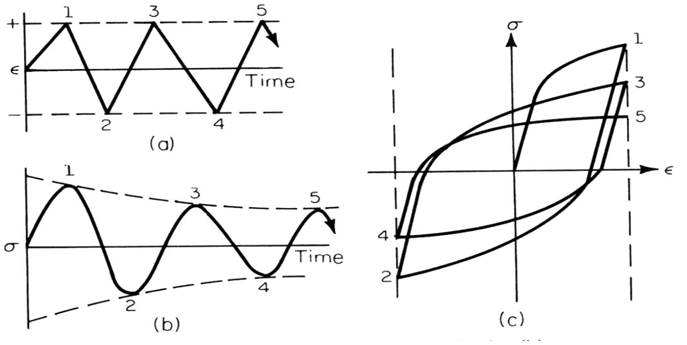

Figure 4-2. Cyclic softening (a) constant strain control, (b) stress response, (c) cyclic stress-strain response.

Cyclic hardening or softening may be predicted from the ratio of monotonic ultimate tensile strength, $\sigma_{uts}$ to 0.2% yield strength, $\sigma_{ys}$ [Manson and Hirschberg 1964]. If $\sigma_{uts}/\sigma_{ys}$ is greater than 1.4, the material will often cyclically harden; if $\sigma_{uts}/\sigma_{ys}$ is less than 1.2, the material will often cyclically soften; if $\sigma_{uts}/\sigma_{ys}$ is between 1.2 and 1.4, the prediction is difficult. The material's cyclic behavior can also be predicted from the monotonic strain hardening exponent, $n$. In general, if $n > 0.2$, the material will cyclically harden; if $n < 0.1$, the material will cyclically soften.

Figure 4-3 shows the tensile curves of G91 steel tested at 20 and 550°C. The alloy shows distinctively different stress-strain behavior at these two temperatures. Significant strain hardening occurred at 20°C, while only limited strain hardening was observed at 550°C. The $\sigma_{uts}/\sigma_{ys}$ is 1.23 at 20°C, and 1.07 at 550°C. Cyclic softening is expected to occur at 550°C, while the alloy may exhibit cyclic softening or hardening at 20°C. In the creep-fatigue experiments performed in this study, cyclic softening occurred throughout the life at 550°C, while slight cyclic hardening was observed in the first 10 cycles, followed by continuous cyclic softening at 20°C.

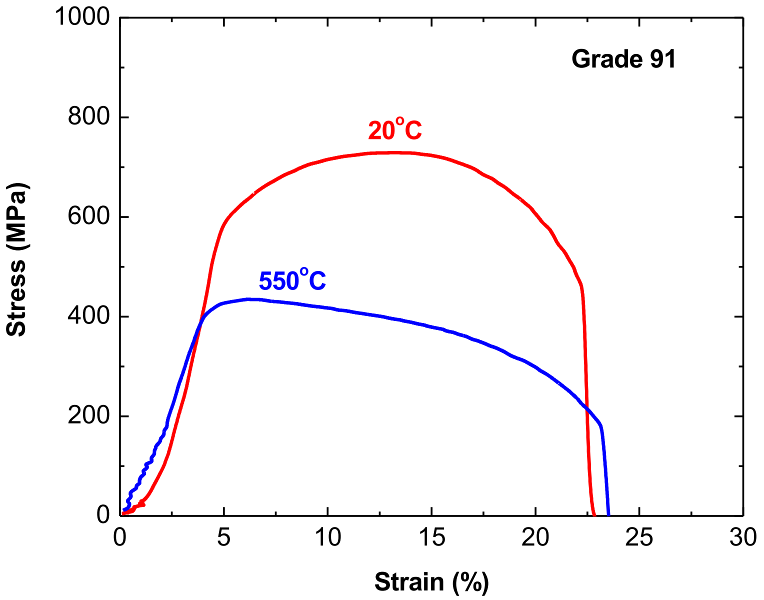

Figure 4-3. Tensile curves of G91 tested at 20 and 550°C.

A Cyclic Softening Model was developed specifically for G91 steel. The model includes contributions of both plasticity and creep deformation. The instantaneous stress level, $\sigma(N)$, at the number of cycle, $N$, is given by:

$$\sigma(N) = \sigma_0 (\varepsilon_p)^k \cdot \left(\frac{1}{N}\right)^m \tag{4-1}$$

where $\sigma_0$ is the stress constant, $\varepsilon_p$ is the plastic strain for each cycle, and $k$, $m$ are the material constants. For a given temperature, $T$ and a total strain range, $\Delta\varepsilon_t$, the value of stress constant, $\sigma_0$, can be obtained from the tensile stress-strain curve of G91 steel. The power exponent, $k$ is assumed the same as the power exponent of strain hardening of the tensile stress-strain behavior. The power exponent, $m$, is determined by the power-law creep, i.e.:

$$\begin{aligned} \dot{\varepsilon} &= A\sigma^n \\ m &= 1/n \end{aligned} \tag{4-2}$$

where $\dot{\varepsilon}$ is the steady-state creep rate, $\sigma$ is the applied stress, and $n$ is the dislocation power-law exponent.

The tensile and creep properties of G91 steel were used in Eqs. (4-1) and (4-2) to predict its cyclic softening behavior. Figure 4-1 shows the calculated cyclic softening curves for a range of total strain ranges, 0.5-1.5% at the test temperature of 550°C. The calculated cyclic stress curves well capture the trends of cyclic softening response of G91 steel: the peak stress decreases with increasing number of cycles, and cyclic softening effect is stronger at a higher total strain range. The calculated cyclic softening curves were compared with the literature data [Kannan et al. 2009, Shankar et al. 2006]. A reasonable agreement was achieved between the experimental data and model predictions.

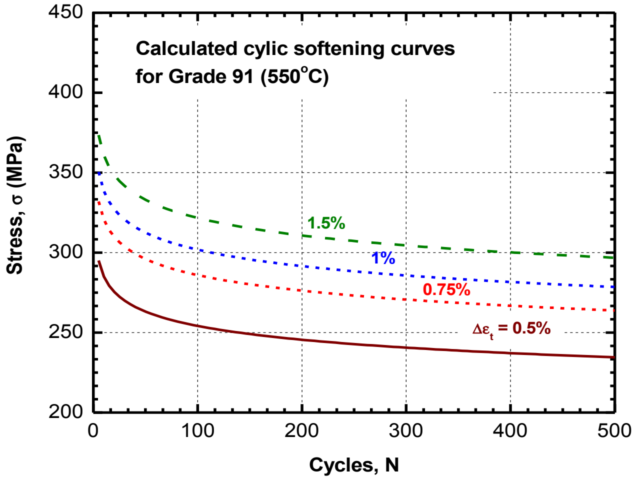

Figure 4-4. Calculated cyclic softening curves for G91 steel for total strain ranges of 0.5–1.5% at 550°C.

The detailed information obtained in the creep-fatigue experiments presented in Section 3 allows further refinement of the Cyclic Softening Model. As shown in Fig. 3-8 and Eq. (3-2), the plastic strain of a cycle follows a power-law relationship with the number of cycles, i.e.:

$$\Delta\varepsilon_p / 2 = p \cdot (N)^q \tag{4-3}$$

Combining Eqs. (4-1) and (4-3), the Cyclic Softening Model can be simplified to the following format:

$$\sigma(N) = B \cdot (N)^{-m'} \tag{4-4}$$

where B and m' are material constants. The cyclic stress profiles shown in Fig. 3-9 were fitted with Eq. (4-4), and the results are shown in Fig. 4-5. The cyclic stress curves can be well described by Eq. (4-4) except the transient stage in the first ten cycles. More specifically, the cyclic stress curves of G91 can be expressed by the following equation:

$$\sigma(N) = 1.1 \cdot \sigma_{(N=1)} \cdot (N)^{-m'} \tag{4-5}$$

where $\sigma_{N=1}$ is the peak stress in the first cycle. The cyclic stress curve for the three creep-fatigue tests are given by:

$$\sigma(N) = 1.1 \cdot \sigma_{(N=1)} \cdot (N)^{-0.064} \quad \text{(550°C, 0.25%, TCH 60s)}$$

$$\sigma(N) = 1.1 \cdot \sigma_{(N=1)} \cdot (N)^{-0.042} \quad \text{(400°C, 0.5%, TCH 60s)}$$

$$\sigma(N) = 1.1 \cdot \sigma_{(N=1)} \cdot (N)^{-0.034} \quad \text{(20°C, 0.5%, TCH 60s)} \tag{4-6}$$

The increase of the power exponent m' with increasing temperature implies that the creep deformation becomes more significant at high temperature.

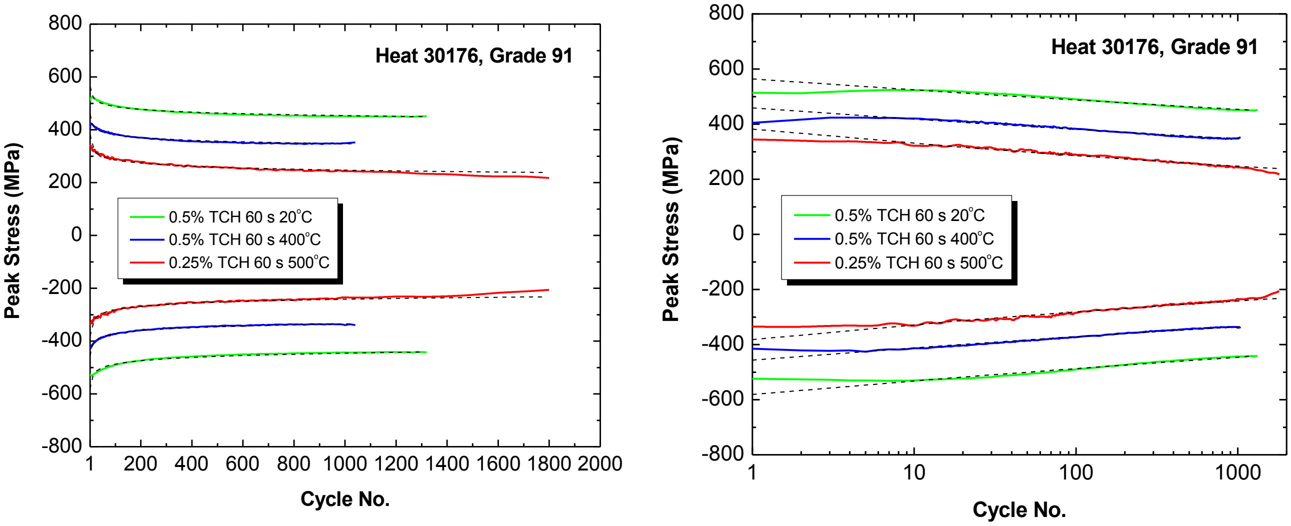

(a) (b)

Figure 4-5. Comparison of the modeled cyclic softening curves with experimental data in (a) linear scale and (b) log scale, for G91 specimens tested at 550°C with total strain amplitude of 0.25%, 400°C with total strain amplitude of 0.5% and 20°C with total strain amplitude of 0.5%, respectively. All three tests were carried out with a hold time of 60 s applied at peak strains in tension and compression (TCH 60 s) in air.

### *4.2 Stress Relaxation Model*

Data of stress relaxation during hold time is critical in evaluating material’s inelastic behavior and deformation characteristics and for estimating creep damage under creep-fatigue conditions. Various approaches have been adopted in evaluating stress relaxation behavior during hold times. In ASME NH, stress relaxation is determined from the isochronous stress-strain curves. This approach has shown over-conservatism in comparison with experimental results [Asayama 2007]. Both the French Code for Liquid Metal Fast Reactor (RCC-MR) and High Temperature Structural Design Guideline for Fast Breeder Demonstration Reactor (DDS) use creep strain curves and the strain hardening law to determine the stress relaxation response, and generally provide a better description of stress relaxation behavior. Overall, all three procedures tend to predict higher stresses than experimental observations [Asayama 2007]. Creep damage calculated from measured stress relaxation curves may give a better knowledge on the creep-fatigue damage.

When a hold time is introduced at maximum tensile position, or minimum compressive position, or combined maximum tensile and minimum compressive positions of a creep-fatigue test, creep will occur during hold time if the tests are run in constant stress control; stress relaxation will occur during hold period if the tests are run in constant total strain control. Figure 4-6 shows continuous cycling and cycling with different types of hold types and stress relaxation during hold in constant total strain control. Stress relaxation during hold produces an additional amount of plastic strain compared to continuous cycling. The increase in plastic strain range can be calculated by the total relaxed stress assuming that unloading is elastic:

$$\Delta\varepsilon_{rp} = \frac{\Delta\sigma_r}{E} \tag{4-7}$$

where $\Delta\varepsilon_{rp}$ is the increase in plastic strain due to relaxation, $\Delta\sigma_r$ is the total relaxed stress during hold, and E is the Young's modulus. The changes of plastic strain rate during hold can also be obtained from stress relaxation curves. During hold time, the total strain range is held constant, and the rate of total strain range is zero, i.e.:

$$\dot{\varepsilon}_{rt} = \dot{\varepsilon}_{re} + \dot{\varepsilon}_{rp} = 0 \tag{4-8}$$

where $\dot{\varepsilon}_{rt}, \dot{\varepsilon}_{re}$ and $\dot{\varepsilon}_{rp}$ are the total strain rate, elastic strain rate and plastic strain rate, respectively. The elastic strain rate can be calculated using Hook's law, and is defined as:

$$\dot{\varepsilon}_{re} = \frac{1}{E}\frac{d\sigma_r}{dt} \tag{4-9}$$

where $\sigma_r$ is instantaneous relaxation stress and t is time. Hence, the plastic strain rate during hold can be obtained by:

$$\dot{\varepsilon}_{rp} = -\dot{\varepsilon}_{re} = -\frac{1}{E}\frac{d\sigma_r}{dt} \tag{4-10}$$

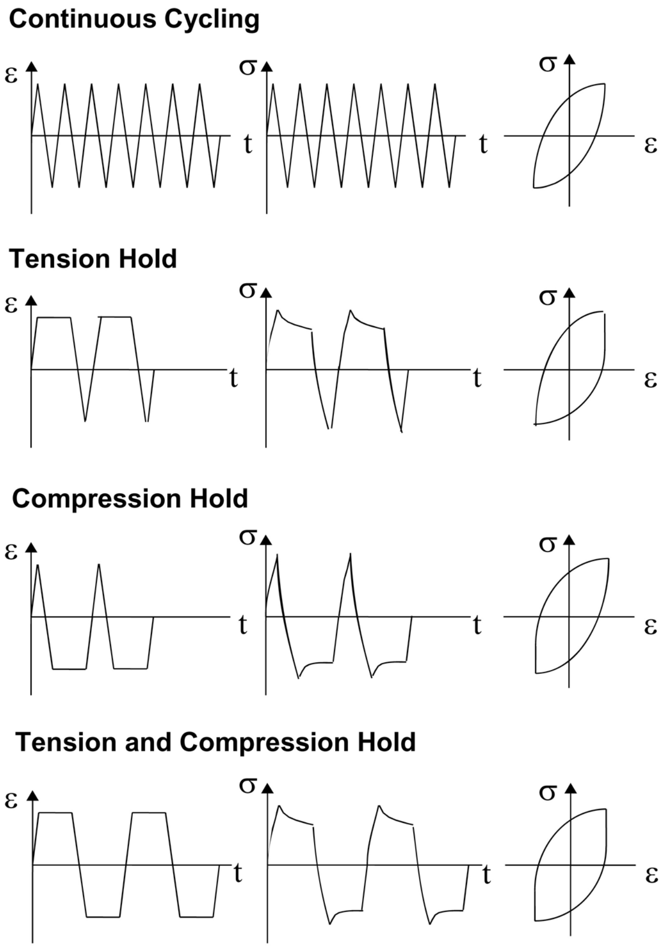
Continuous Cycling
ε
t
σ
t
σ
ε
Tension Hold
ε
t
σ
t
σ
ε
Compression Hold
ε
t
σ
t
σ
ε
Tension and Compression Hold
ε
t
σ
t
σ
ε

Figure 4-6. Stress relaxation during hold time.

Due to the cyclic softening effect in G91 steel, the stress relaxation responses during hold time vary with the number of cycles during the entire cyclic process. As shown in Figs. 3-10 to 3-12, cyclic softening has a strong effect on the stress relaxation response. The initial stress at the beginning of the hold time is reduced significantly with increasing number of cycles, resulting in subsequently lower relaxed stress at a given time during hold at different cycles.

In fiscal year 2010, we recovered stress relaxation data from thirteen creep-fatigue tests conducted at Oak Ridge National Laboratory in the late 1980s and early 1990s, and conducted extensive analysis of the test data. Based on this database and available literature data, we have developed a Stress Relaxation Model specifically applied to G91 steel. The model was based on the modified Feltham stress relaxation equation [Feltham 1961]. The inelastic strain rate during hold is expressed by:

$$\dot{\varepsilon}_{in} = A'\left[\sigma_{r(t=0)}\right]^{n'}(\beta t + 1)^{-1} \tag{4-11}$$

where $\sigma_{r(t=0)}$ is the initial stress of stress relaxation, $\beta$, $A'$ and $n'$ are the constants. The relaxed stress during hold time can then be determined by:

$$\sigma_r(t) = \sigma_{r(t=0)} - \frac{EA'[\sigma_{r(t=0)}]^{n'}}{\beta}\ln(\beta t + 1) \tag{4-12}$$

where $\sigma_r(t)$ is the relaxed stress at time, $t$ during hold.

The stress relaxation curves obtained in the three creep-fatigue experiments conducted at 20, 400 and 550°C were modeled using Eq. (4-12). It was found that the normalized stress relaxation curves have little dependence on the number of cycles. The normalized stress relaxation curves can be described by a simplified form:

$$\frac{\sigma_r(t)}{\sigma_{r(t=0)}} = 1 - \alpha\ln(\beta t + 1) \tag{4-13}$$

The stress relaxation curves for the three creep-fatigue tests can be described by the following functions:

$$\frac{\sigma_r(t)}{\sigma_{r(t=0)}} = 1 - 0.053\ln(2t + 1) \quad \text{(550°C, 0.25\%, TCH 60s)}$$

$$\frac{\sigma_r(t)}{\sigma_{r(t=0)}} = 1 - 0.018\ln(12t + 1) \quad \text{(400°C, 0.5\%, TCH 60s)}$$

$$\frac{\sigma_r(t)}{\sigma_{r(t=0)}} = 1 - 0.008\ln(71t + 1) \quad \text{(20°C, 0.5\%, TCH 60s)} \tag{4-14}$$

Modeled stress relaxation curves are compared with the experimental data in Figs. 4-7 to 4-9 for the tests at 20, 400 and 550°C, respectively. A good agreement is achieved for all three test conditions.

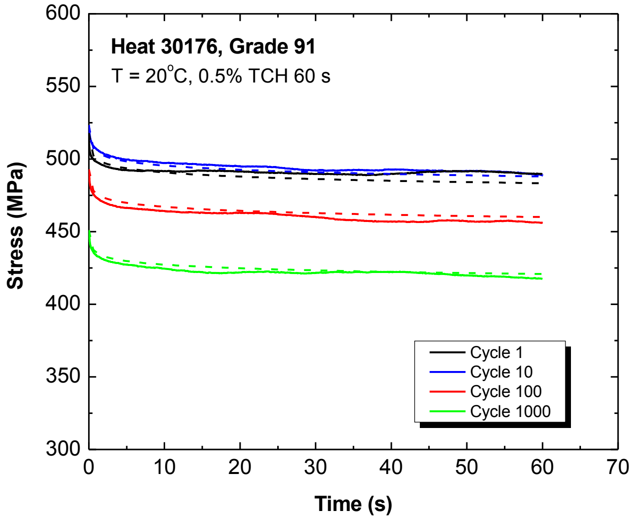

Figure 4-7. Comparison of modeled stress relaxation curves with experimental data for cycles 1, 10, 100, and 1000 for G91 tested at 20°C, 0.5% total strain amplitude with a tension and compression hold time of 60 s.

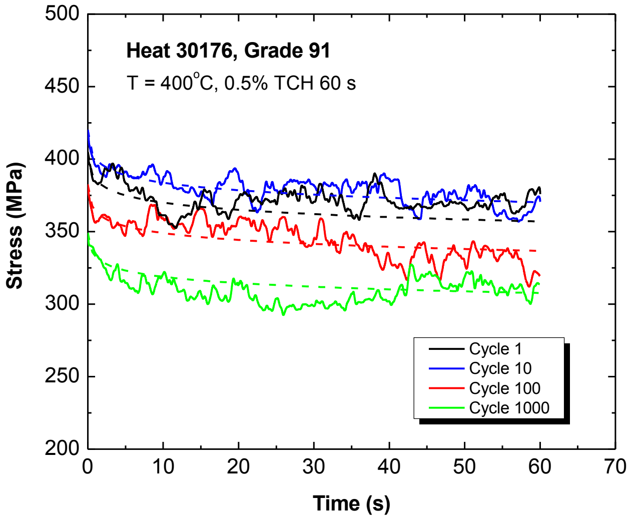

Figure 4-8. Comparison of modeled stress relaxation curves with experimental data for cycles 1, 10, 100, and 1000 for G91 tested at 400°C, 0.5% total strain amplitude with a tension and compression hold time of 60 s.

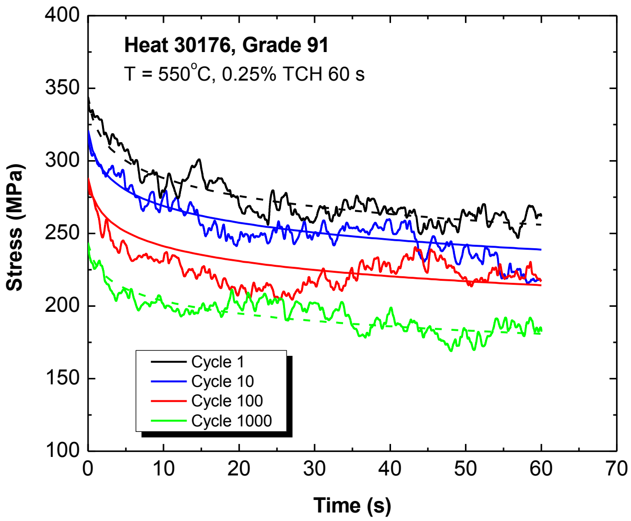

Figure 4-9. Comparison of modeled stress relaxation curves with experimental data for cycles 1, 10, 100, and 1000 for G91 tested at 550°C, 0.25% total strain amplitude with a tension and compression hold time of 60 s.

### *4.3 Improved Bilinear Creep-Fatigue Damage Model*

The creep-fatigue damage in G91 steel was evaluated using the bilinear damage method as adopted by ASME Subsection NH [2011]. Improvements were made by taking into account the cyclic history and cyclic softening effect. The average fatigue life curves and average creep rupture curves were used in the evaluations without any safety margins. The hold-time stress relaxation data were modeled and the simulated stress relaxation curves were used in the assessment of the unit creep damage per cycle.

The unit creep damage per cycle under creep-fatigue loading, $d_c$ is calculated by:

$$d_c = \int_0^{t_h} \frac{dt(\sigma)}{t_R(\sigma)} \tag{4-15}$$

where $t_h$ is the length of the hold time, $t_R(\sigma)$ is the creep rupture life at a given stress level, $\sigma$. The unit fatigue damage per cycle under creep-fatigue loading, $d_f$ is calculated by:

$$d_f = \frac{1}{N_f} \tag{4-16}$$

where $N_f$ is the cycle to failure under pure fatigue at a given strain range. The total creep-fatigue damage, $D$ is given as:

$$\begin{aligned} &D = D_f + D_c; \\ &D_f = N_{cf} \cdot d_f; \\ &D_c = N_{cf} \cdot d_c \end{aligned} \tag{4-17}$$

where $D_f$ is the total fatigue damage, $D_c$ is the total creep damage, and $N_{cf}$ is the cycle to failure under creep-fatigue loading.

The data required in the calculations of creep-fatigue damage include the strain–fatigue life data under continuous cycling, creep stress–rupture life data, and the stress relaxation data during hold time of a creep-fatigue cycle. There is a large database of the pure fatigue data and creep rupture data for G91 steel in the literature. This database was used in the calculations of the bilinear creep-fatigue damage. Data was collected on five commercial heats (heat No. 10148, 30176, 30394, 30383, and 91887) of G91 steel, tested by the Oak Ridge National Laboratory in the late 1980's and early 1990's [Blass et al 1989, 1990, 1991, 1992]. The available fatigue data under continuous cycling at 538 and 593°C are compiled and plotted in Fig. 4-10. These fatigue tests were performed in air under the constant total strain range in the strain control mode with R = -1 and the strain rate of 0.004 $s^{-1}$. No significant temperature dependence of the fatigue life was observed in this temperature range (538-593°C). The strain-life relation can be expressed by:

$$\Delta\varepsilon = 0.6 \cdot \left(N_f\right)^{-0.06} + 74 \cdot \left(N_f\right)^{-0.65} \tag{4-18}$$

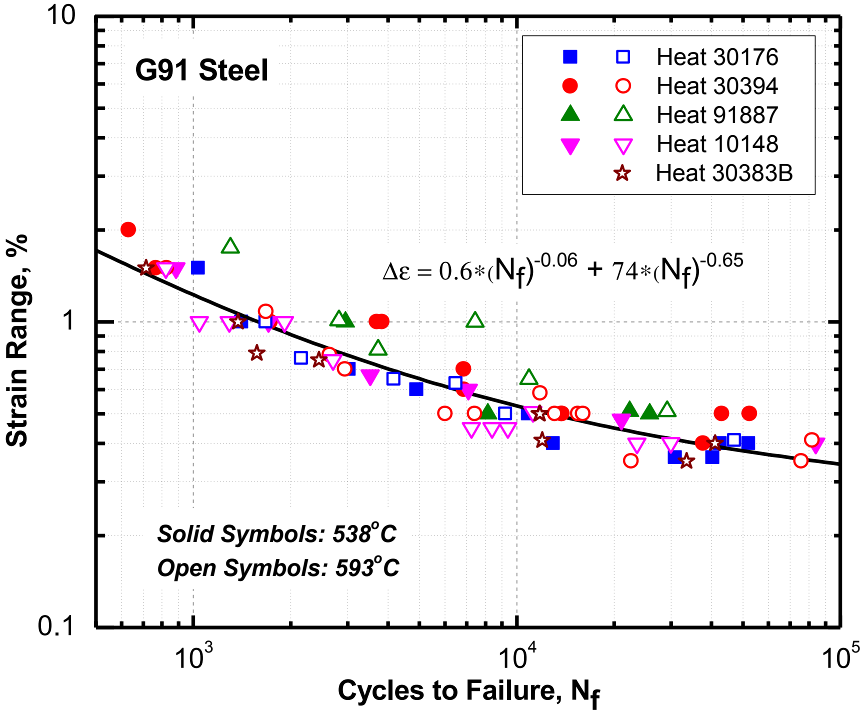

Figure 4-10. Compilation of the fatigue data in terms of the total strain range and the cycle to failure under continuous cycling for five commercial heats of G91 steel tested at 538 and 593°C in air. Tests were performed at Oak Ridge National Laboratory. Data were taken from the literature. The solid line represents the average strain-life relation.

The available creep rupture data for the five heats of G91 steel tested at 538 and 593°C are compiled and plotted in Fig. 4-11. Distinct creep rupture behavior was observed at these two temperatures. At 538°C, the stress-rupture life curve can be described by a single power-law relation, while the stress-rupture life curve at 593°C shows a deflection at the stress level of ~140 MPa, below which the rupture time decreases more rapidly with increasing stress.

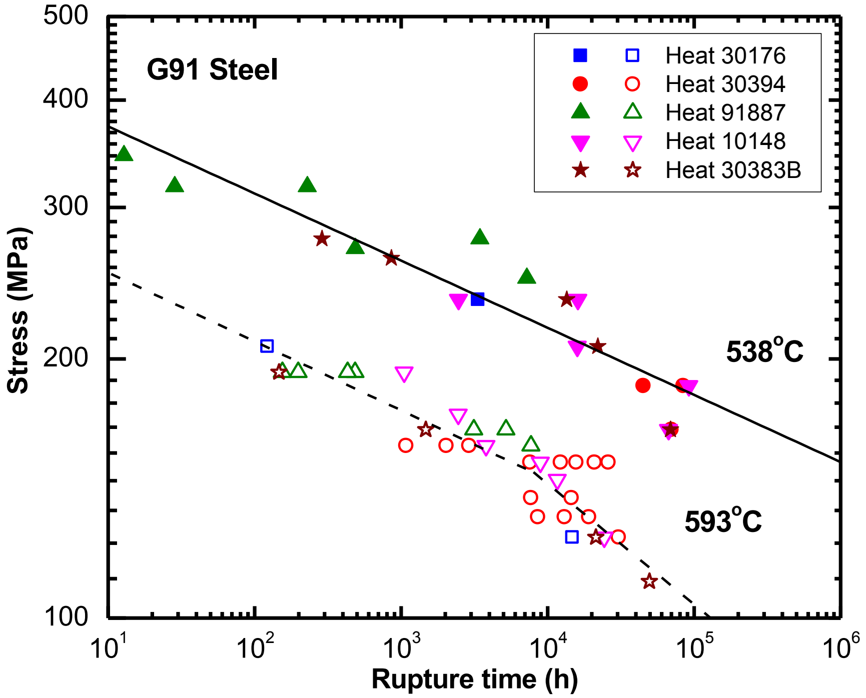

Figure 4-11. Compilation of the creep rupture data in terms of the applied stress and the rupture life for five commercial heats of G91 steel tested at 538 and 593°C in air. Tests were performed at Oak Ridge National Laboratory. Data were taken from the literature. The solid lines represent the average creep rupture behavior.

The stress relaxation data recovered in the past year from the thirteen creep-fatigue tests conducted at Oak Ridge National Laboratory in late 1980s and early 1990s allowed evaluation of G91 creep-fatigue damage using improved bilinear creep-fatigue damage model. Evaluation was performed on 11 creep-fatigue tests. The unit creep damage per cycle under hold-time creep-fatigue loading, $d_c$ was calculated using the average creep rupture curves and experimentally obtained hold-time stress relaxation data. The tension hold and compression hold was treated in the same manner. Because only the stress relaxation data of the first (or second) cycle, 10th cycle, 100th cycle, and the half-life were available in digital form, the unit creep damage was calculated for these cycles only. Figure 4-12 shows the unit creep damage as a function of the number of cycles for the creep-fatigue tests conducted at 538°C. The unit creep damage changed continuously with cycling. A lower relaxed stress at a higher cycle due to cyclic softening resulted in a decreased unit creep damage. The creep damage for the cycle at the half-life can be 2 orders of magnitude lower than the damage in the first cycle. While a number of variables including heat variations, strain range, hold type, and hold time are involved in the tests given in Fig. 4-12, the length of the hold time is apparently a critical factor in determining the amount of unit creep damage. As the hold time increased from 15 minutes to 30 minutes, the unit creep damage became significantly higher.

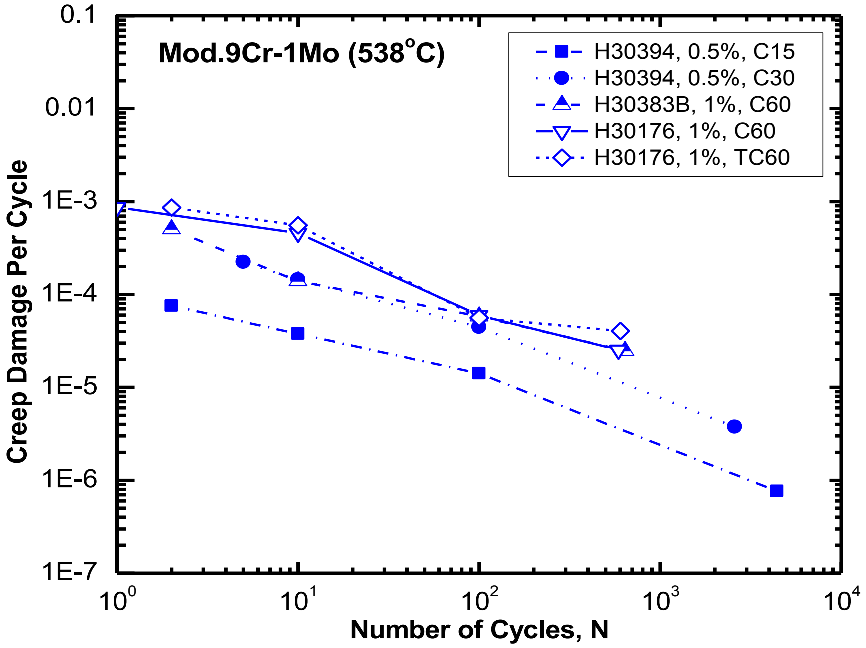

Figure 4-12. Unit creep damage as a function of the number of cycles for G91 steel tested in creep-fatigue conditions at 535°C (C60–compression hold for 60 min, T60–tension hold for 60 min, and TCH60–tension and compression hold for 60 min).

The unit creep damage per cycle under creep-fatigue loading at 593°C was calculated and plotted as a function of the number of cycles in Fig. 4-13. Again, the creep damage for each cycle continuously decreased with increasing number of cycles. Among various factors of different heats, strain range level, hold type, and hold time, the hold type, i.e. either hold in tension or in compression, seems to play the most important role in determining the extent of creep damage. The hold in compression gives rise to significantly higher damage than the hold in tension.

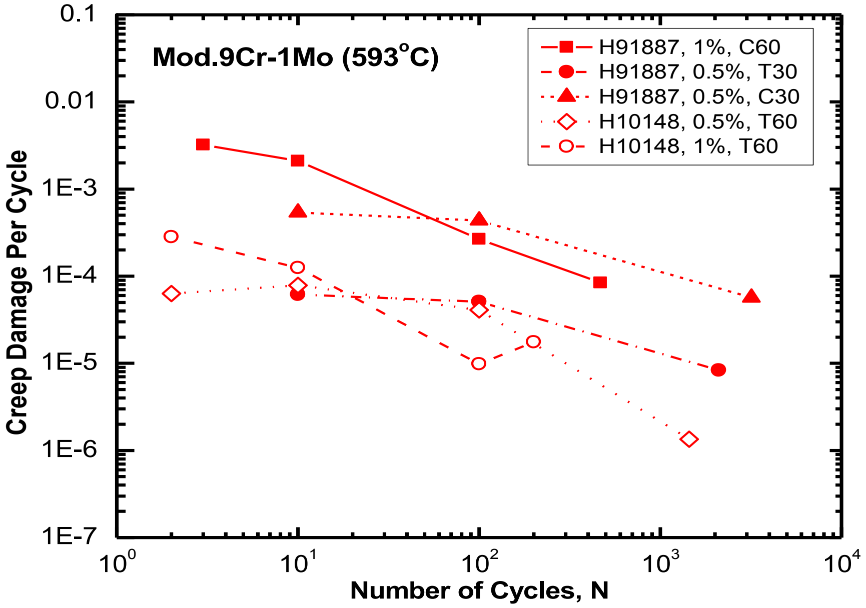

Figure 4-13. Unit creep damage as a function of the number of cycles for G91 steel tested in creep-fatigue conditions at 593°C.

The creep damage rate and the accumulation of creep damage as a function of time during hold are shown in Fig. 4-14. The creep damage rate is the highest at the beginning of the hold, and then decreases rapidly with increasing hold time after the first second. The creep damage rate at the end of the hold (3600 s) is about three orders of magnitudes lower than the initial value. The rate of creep damage accumulation continuously decreased with increasing time, but no apparent saturation was observed up to one-hour hold time.

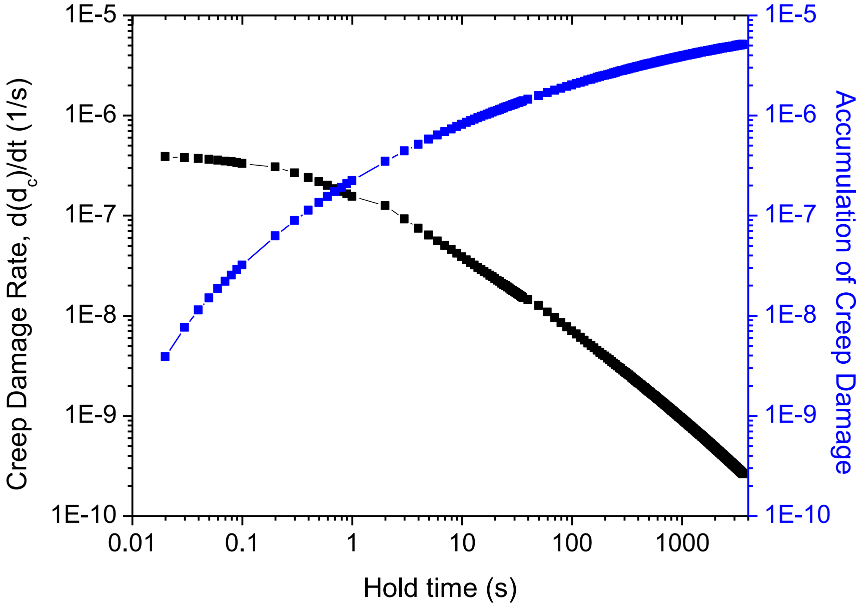

Figure 4-14. An example showing the creep damage rate and the accumulation of creep damage as a function of hold time per unit cycle for G91 steel.

The creep-fatigue interaction diagrams were constructed using Eqs. (4-15) to (4-17), and shown in Figs (4-15) to (4-17). The ASME creep-fatigue damage envelope for G91 steel, along with the intersection of (0.01, 0.1), is shown by the dashed lines. The fatigue damage was calculated using the average fatigue life curve given in Fig. 4-10. The fatigue damage falls in the range of 0.2–1, and the damage at 593°C is generally lower than that at 538°C. The creep damage can be drastically different, depending on the unit creep damage used in the calculations. In Fig. 4-15, the total creep damage was calculated using the unit creep damage at the half-life, multiplied by the number of cycles to failure; in Fig. 4-16 the total creep damage calculated using the unit creep damage at cycle 10, multiplied by the number of cycles to failure. When the unit creep damage at half-life was used in the calculations, a majority of the creep-fatigue tests show creep damage below 0.1. The lowest total creep damage was ~0.004, and the highest ~0.36. Two tests fall inside the ASME envelope. However, when the unit creep damage at cycle 10 was used in the calculations, the creep damage was almost one order of magnitude higher than the damage calculated by the half-life data for the same creep-fatigue tests. The lowest total creep damage was ~0.05, and the highest ~3.4. All the tests are outside the ASME envelope. The evaluation of the total creep damage shown in Fig. 4-17 takes into account of the cyclic history, and was calculated in the following way:

$$D_c = \int_1^{N_{cf}/2} d_c + d_c(HL) \times N_{cf}/2 \tag{4-19}$$

where $d_c(HL)$ is the unit creep damage at the half-life. The first term in Eq. (4-19) was calculated by integration of the data (unit creep damage per cycle versusnumber of cycles curves) given in Figs. 4-12 and 4-13. This calculation accounts for the creep damage up to the half-life, and represents more closely to the actual damage. It is seen that all the creep-fatigue tests are located outside the ASME envelope. The smallest creep damage is ~0.01, and the highest ~1.

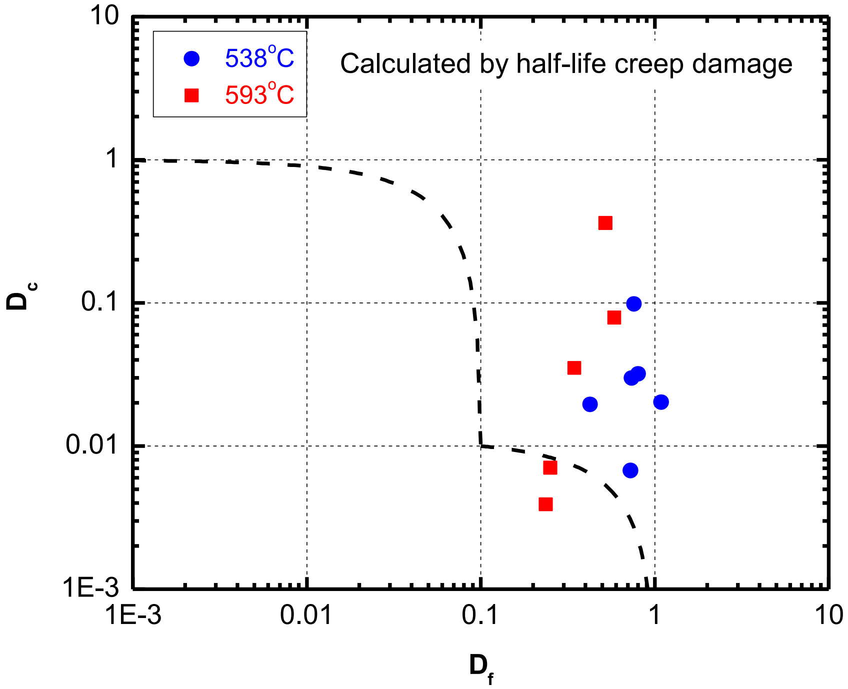

Figure 4-15. Creep-fatigue interaction diagram calculated using the unit creep damage at the half-life for G91 steel. The dash lines represent the ASME creep-fatigue damage envelope for G91 steel with the intersection of (0.01, 0.1).

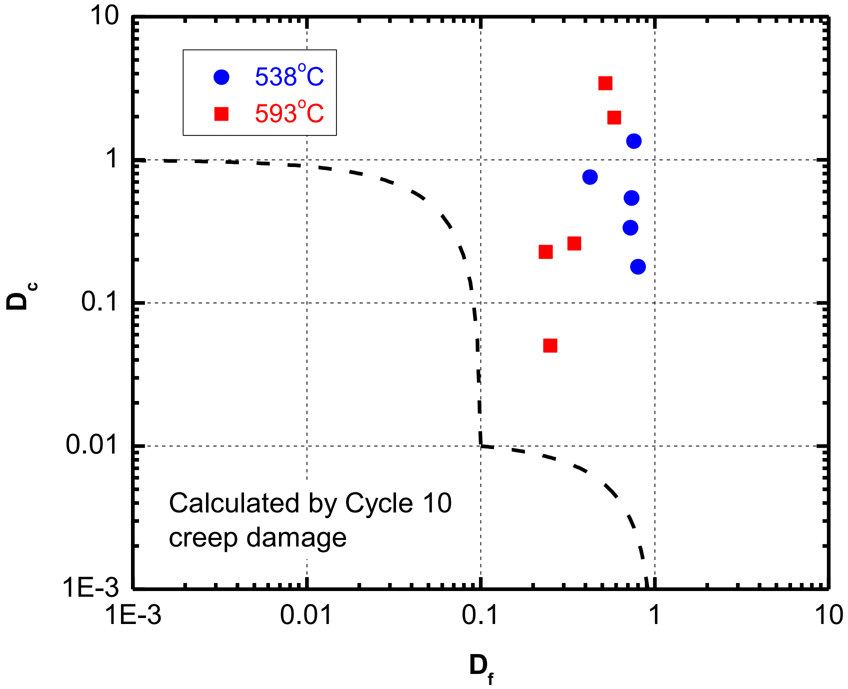

Figure 4-16. Creep-fatigue interaction diagram calculated using the unit creep damage at cycle 10 for G91 steel. The dash lines represent the ASME creep-fatigue damage envelope for G91 steel with the intersection of (0.01, 0.1).

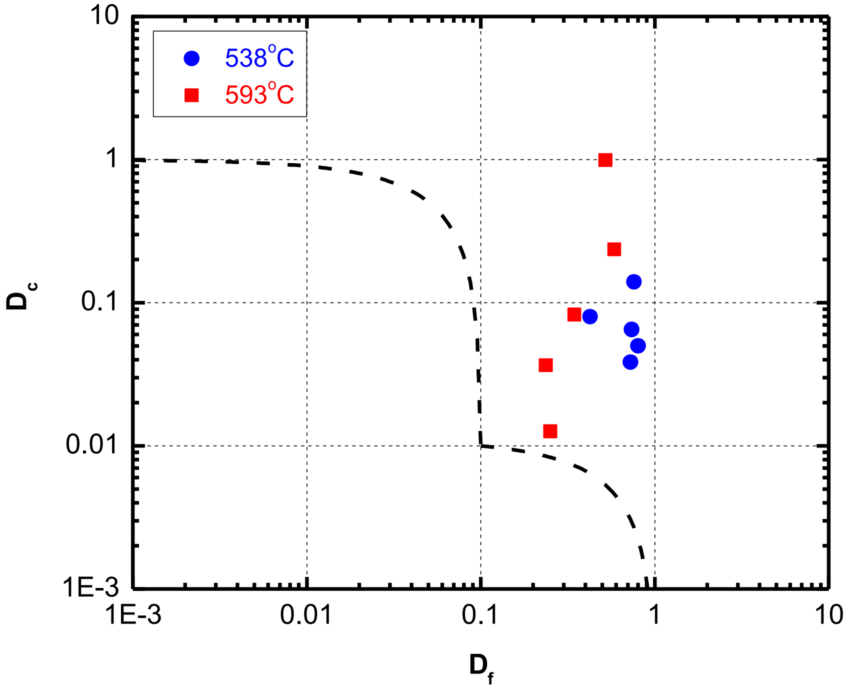

Figure 4-17. Creep-fatigue interaction diagram calculated by integration of unit creep damage vs. cycles curves for G91 steel. The dash lines represent the ASME creep-fatigue damage envelope for G91 steel with the intersection of (0.01, 0.1).

The above assessment reveals that the estimation of total creep damage is strongly dependent on the history of cycling and stress relaxation response in each cycle of a creep-fatigue test. When the stress relaxation curves at the 10th cycle were used in the evaluation of creep-fatigue damage, the calculated creep damage can be one order of magnitude higher than that calculated using the unit creep damage at the half-life. The initial stress of relaxation is a critical factor in determining the unit creep damage for a given cycle, and it must be determined accurately to ensure the reliability of the creep-fatigue damage assessment. This is particularly important for G91 steel, which exhibits remarkably cyclic softening behavior during cycling. The assessment of creep-fatigue damage also requires an accurate description of the stress relaxation response during hold time of a creep-fatigue cycle such that the creep damage associated with stress relaxation can be determined with confidence.

The cyclic softening behavior of G91 steel can be well captured by the Cyclic Softening Model, and the stress relaxation behavior during hold can be well described by the Stress Relaxation Model, as presented in Sections 4.1 and 4.2. The Cyclic Softening Model, Stress Relaxation Model, and Bilinear Creep-Fatigue Damage Model can be integrated into a powerful framework to predict the lifetime of a material under creep-fatigue loading. As shown in Eq. (4-5), the peak stress for each cycle can be determined by the peak stress in the first cycle (or tensile property). The stress relaxation curve for the given cycle can then be established by Eq. (4-13) with the known peak stress. When Eqs. (4-5) and (4-13) are combined, the stress relaxation curve for a given cycle can be expressed by:

$$\sigma_r(t,N) = (c \cdot \sigma_0 \cdot N^{-m'}) \cdot \left(1 - \alpha \ln(\beta t + 1)\right) \tag{4-20}$$

where $\sigma_0$ is the peak stress in the first cycle, and c, m', α, β are the material constants. For the creep-fatigue test conducted at 550°C, 0.25% total strain amplitude with a tension and compression hold time of 60 s, Eq. (4-20) becomes:

$$\sigma_r(t,N) = (1.1 \cdot \sigma_0 \cdot N^{-0.064}) \cdot \left(1 - 0.053\ln(2t+1)\right) \tag{4-21}$$

According to Fig. 4-10, the creep rupture curve at 538°C can be expressed by:

$$\sigma = 446 \cdot (t_R)^{-0.078} \tag{4-22}$$

where σ is the applied stress, and $t_R$ is the creep rupture life. The unit creep damage per cycle can be calculated for every cycle using Eqs. (4-21), (4-22), and (4-15). The bilinear creep-fatigue damage can then be evaluated using Eqs. (4-16) and (4-17). It is important to note that the cyclic softening and consecutive stress relaxation responses can be considered for the entire cyclic process in the model calculation. While the framework is promising, it must be recognized that it was based primarily on three creep-fatigue tests performed in this study. The models must be validated and further improved by a large number of well-designed creep-fatigue experiments that cover a wide range of variables such as temperature, strain amplitude, waveform, strain rate, hold time, etc.

### *4.4 Interactive Damage Rate Model*

While the improved bilinear creep-fatigue damage model provides better assessment of creep-fatigue damage in G91 steel, it doesn't have a physical basis that captures the unique deformation and failure process in high-strength ferritic/martensitic steel such as G91 under creep-fatigue loading. Other creep-fatigue predictive approaches, empirical or mechanistic, must be evaluated to develop a model that is uniquely applicable to this class of alloys.

The Damage Rate Model has been successfully applied in several materials, e.g. Type 304 austenitic stainless steel and 2.25Cr-1Mo ferrtic steel, to predict the creep-fatigue behavior under various loading conditions [Majumdar and Maiya 1978, 1979, 1980, 1981]. The applicability of this model to G91 steel has not been evaluated, and is explored in this program.

A single rate equation was initially proposed by Majumdar and Maiya [1978] to account for fatigue crack growth in the Damage Rate Model. The Model was later modified to take into account the grain boundary cavitation under hold time during cycling. The Model was further modified to take into account the interactive process of fatigue-induced crack growth and creep-induced grain boundary cavitation, so-called "Interactive Damage Rate Equation." The Interactive Damage Rate Equation is given as:

$$\frac{1}{a}\frac{da}{dt} = \begin{Bmatrix} T \\ C \end{Bmatrix} (1 + \alpha \ln c / c_o) |\varepsilon_{in}|^m |\dot{\varepsilon}_{in}|^k \tag{4-23}$$

where:
$a$ = current crack length,
$\varepsilon_{in,}\dot{\varepsilon}_{in}$ = current total inelastic strain as measured from last reversal and inelastic strain rate, respectively,
$c_o$ and $c$ = initial and current cavity sizes, respectively
$T$, $C$, $\alpha$, $m$, $k$ = material parameters.

"Failure" is assumed to occur either by the growth of a crack or by the coalescence of cavities, and failure occurs when the crack length reaches a value of $a_f$ or cavity size reaches a value of $c_f$, whichever occurs earlier.

The fatigue life can be determined by the integration of Eq. (4-23). For symmetric continuous cycling at zero mean stress and a given strain rate, the fatigue life, $N_f$ is given as:

$$N_f = \frac{m+1}{2A}\left(\Delta\varepsilon_{in}\right)^{-(m+1)}\dot{\varepsilon}_{in}{}^{1-k} \tag{4-24}$$

and

$$A = \frac{T+C}{2} / \ln\frac{a_f}{a_o} \tag{4-25}$$

where:
$\Delta\varepsilon_{in}$ = total inelastic strain range,
$a_o$ = initial length of a crack,
$a_f$ = final crack size.

For the case of slow-fast loading (slow tensile and fast compressive) with an average slow tensile inelastic strain rate $\dot{\varepsilon}_s$, and an average fast compressive inelastic strain rate $\dot{\varepsilon}_f$, the fatigue life is given as:

$$D_T = \frac{1}{m+1}\left(\Delta\varepsilon_{in}\right)^{m+1}\left[C_T\dot{\varepsilon}_s^{k-1} + C_C\dot{\varepsilon}_f^{k-1}\right] \tag{4-26}$$

and

$$D_C = \frac{A_g}{m+1}\left(\Delta\varepsilon_{in}\right)^{m+1}\left[\dot{\varepsilon}_s^{k_c-1} - \dot{\varepsilon}_f^{k_c-1}\right] \tag{4-27}$$

and

$$N_f = \left[-1 + \left\{1 + \frac{2D_C}{D_T}\right\}^{1/2}\right] / D_C \tag{4-28}$$

For the case of fast-slow loading with an average fast tensile inelastic strain rate $\dot{\varepsilon}_f$ and an average slow compressive inelastic strain rate $\dot{\varepsilon}_s$, $D_C = 0$,

$$D_T = \frac{1}{m+1}\left(\Delta\varepsilon_{in}\right)^{m+1}\left[C_T\dot{\varepsilon}_f^{k-1} + C_C\dot{\varepsilon}_s^{k-1}\right] \tag{4-29}$$

For hold-time cycles with the inelastic strain range, $\Delta\varepsilon_{in}$, the hold time $t_T$ at the peak tensile limit, the hold time $t_C$ at the peak compressive limit, the following equations may be written, if the incremental plastic strain during hold is considered negligible in comparison with the plastic strain range during the ramp:

$$D_T = \frac{C_T + C_C}{m+1}\left(\Delta\varepsilon_{in}\right)^{m+1}\hat{\dot{\varepsilon}}_{in}^{k-1} + C_T\left(\Delta\varepsilon_{in}\right)^{m}\int_o^{t_T}\left|\dot{\varepsilon}_{in}(t)\right|^{k} dt \ + C_C\left(\Delta\varepsilon_{in}\right)^{m}\int_o^{t_C}\left|\dot{\varepsilon}_{in}(t)\right|^{k} dt \qquad (4\text{-}30)$$

and

$$D_C = A_g\left(\Delta\varepsilon_{in}\right)^{m}\left[\int_o^{t_T}\left|\dot{\varepsilon}_{in}(t)\right|^{k_c} dt - \int_o^{t_C}\left|\dot{\varepsilon}_{in}(t)\right|^{k_c} dt\right] \qquad (4\text{-}31)$$

where $\dot{\varepsilon}_{in}(t)$ represents the inelastic strain rate during hold.

In an earlier report [Li et al. 2010], we presented a preliminary evaluation of the applicability of the Interactive Damage Rate Model to G91 steel. A set of creep and fatigue data under different temperatures, strain rates, and waveforms from the literature, was used to determine the material parameters in the model. The material parameter, *k*, *m, A* were determined from a least-squares fit of the continuous fatigue data to the crack-growth equation. The material parameter, $C_T$, $C_C$ were determined under the assumption that $T = 2C$. The material parameter, $k_c$ was estimated using the creep rupture data at 550 and 600°C for G91 steel. The parameter, $A_g$ was obtained from the best fit of the fatigue data under slow-fast cycling. The fatigue life under hold-time cyclic loading was predicted for G91 steel using the established Interactive Damage Rate Model, and modeling results are compared with the literature experimental data for the steel tested under constant strain amplitude at a strain rate of 0.005 $s^{-1}$ with a tension hold time of 0.1 h or 1 h at 550 and 600°C in air. This preliminary evaluation showed that the predicted lives are all within a factor of 2 of the observed lives with one exception for a 550°C test.

While this initial attempt was successful and encouraging, a number of issues were identified in developing the Interactive Damage Rate Model for G91 steel. It was noted that several assumptions/simplifications must be made in modeling creep-fatigue damage. For instance, the data of the inelastic strain range and inelastic strain rate during hold are generally not available from previous creep-fatigue experiments, except for the half-life. The half-life data were used in the evaluation of the entire creep-fatigue process, which significantly reduces the accuracy of the modeling results. An assumption of a constant inelastic strain rate during hold had to be made due to lack of stress relaxation data, which may undermine the contributions of plastic deformation during hold time in the overall creep-fatigue damage. Furthermore, the majority of creep-fatigue data in the literature showed no grain boundary cavitation, while grain boundary damage was indeed observed in the creep-fatigue tests at high temperatures. Whether or not the classical creep-fatigue damage mode occurs in G91 steel remains to be clarified, which in turn determines the proper creep-fatigue model that is applicable to this class of materials.

# 5 Accelerated Creep-Fatigue Testing Methodology

Development and validation of reliable and accurate creep-fatigue models demand well-controlled, model-oriented experiments to provide high-fidelity experimental data. The inadequate creep-fatigue database has limited the development of advanced creep-fatigue models and design rules for G91 steel. Previous creep-fatigue experiments focused on providing testing data for qualification of the material, which often have insufficient experimental details that are required for a deeper understanding of deformation and damage mechanisms, optimization of key materials parameters, and validation of models. There is an apparent need that experiments are designed and conducted specifically for model development and validation. The extended service life of nuclear reactor components also calls for an accelerated testing approach to properly assess the performance of reactor materials and components in real nuclear reactor environments.

We propose a methodology that uses known short-term material properties to predict the life under extended hold-time creep-fatigue loading. The concept of the methodology is illustrated in Fig. 5-1. Key material parameters in the creep-fatigue model will be determined by creep properties and fatigue data obtained under symmetric continuous cycling (fast-fast and slow-slow) and asymmetric cycling (slow-fast and fast-slow). Cycling with slow-fast, fast-slow, and slow-slow waveforms often leads to accelerated creep-fatigue damage that is observed under hold-time creep-fatigue loading [Majumdar and Maiya 1981]. Continuous fatigue with various wave-shapes and strain rates may be used as an accelerated approach to simulate the damage. A model can be established based on creep and fatigue properties, and then be used to predict the life under creep-fatigue loading with hold-time in either tension or compression or under combined tension and compression, and validated by the hold-time creep-fatigue data.

.

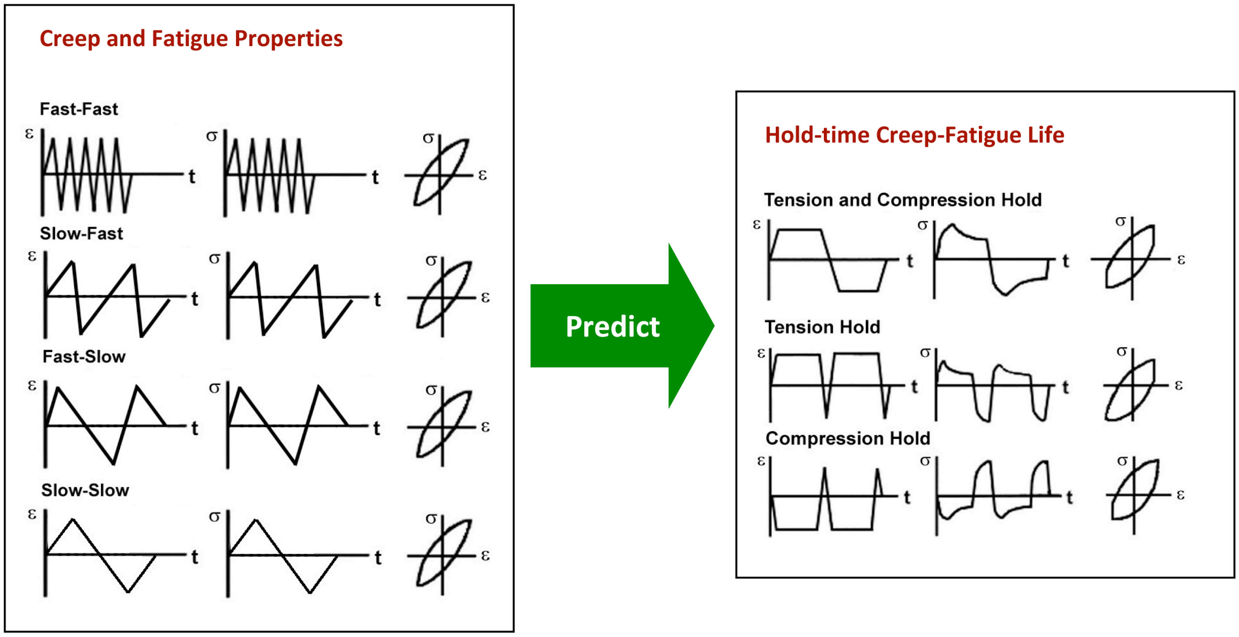
Creep and Fatigue Properties
Fast-Fast
Slow-Fast
Fast-Slow
Slow-Slow
ε
σ
t
Predict
Hold-time Creep-Fatigue Life
Tension and Compression Hold
Tension Hold
Compression Hold

Figure 5-1. Accelerated creep-fatigue damage testing methodology.

# 6 Summary and Future Work

In earlier reports, we have identified a critical need in developing mechanism based creep-fatigue interaction models for life prediction, reliable data extrapolation and a robust design methodology. Recognizing that the current ASME design rule of bilinear damage summation puts severe limits of fatigue and creep loads for G91 steel, the lead structural material in fast reactors, we focus on the creep-fatigue damage issue for G91 steel in the current effort, and will extend it to advanced high-strength ferritic/martensitic steels such as G92 steel.

To support the predictive model development and resolve the over-conservative issue with the ASME design rule for G91 steel, we recovered stress relaxation data from thirteen creep-fatigue tests conducted at Oak Ridge National Laboratory in the late 1980s and early 1990s, and conducted extensive data analysis in fiscal year 2010. Based on this database and available literature data, we have developed a Cyclic Softening Model and a Stress Relaxation Model specifically applied to G91 steel. The Cyclic Softening Model describes the cyclic stress variation as a function of cycle number during creep-fatigue loading, and well captures the cyclic softening effect in G91 steel. The Stress Relaxation Model predicts the stress relaxation curve during the hold time of cyclic loading, and its dependence on the cyclic softening effect of G91 steel.

Two creep-fatigue test systems have been set up to conduct model-oriented creep-fatigue experiments. Results from three creep-fatigue experiments on Heat 30176 of G91 steel are presented in the report: (1) a test performed at 550°C with total strain amplitude of 0.25% and a hold time of 60 s applied at peak strains in both tension and compression, (2) a test performed at 400°C with total strain amplitude of 0.5% and a tension and compression hold time of 60 s, and (3) a test performed at 20°C with total strain amplitude of 0.5% and a tension and compression hold time of 60 s. Three different test temperatures were chosen for two primary reasons: to determine the transition temperature of creep-fatigue interaction from a plasticity-dominated process to a creep-dominated process; to develop unified creep-fatigue models applicable for a wide range of temperatures. With the detailed information obtained in the creep-fatigue experiments, we have further refined the Cyclic Softening Model and Stress Relaxation Model.

The Cyclic Softening Model and Stress Relaxation Model were incorporated into the Bilinear Creep-Fatigue Damage Model, forming a powerful framework for the life prediction by an improved creep-fatigue evaluation methodology. The cyclic softening and consecutive stress relaxation responses in G91 steel can be considered for each cycle of the entire cyclic process in the model calculation. The creep-fatigue damage in G91 steel was evaluated using the improved Bilinear Creep-Fatigue Damage Model without any safety margins. It was found that due to the significant cyclic softening in G91 steel, the unit creep damage in each cycle decreased continuously with increasing number of cycles. This continuous change in creep damage with cycling has significant implication in the evaluation of the total creep-fatigue damage. The total creep damage can be one order of magnitude lower when the unit creep damage at half-life was used in the evaluation in comparison with the calculations using the unit creep damage at cycle 10. An important conclusion was that the accurate assessment of the creep-fatigue damage in G91 steel must consider the history of cycling. This analysis provided the more realistic assessment of creep-fatigue damage and identified critical factors that must be considered in future advanced models for high-strength ferritic/martensitic alloys.

An accelerated creep-fatigue testing methodology was proposed for the design of model-oriented experiments to guide and validate model developments. Future work will focus on creep-fatigue experiments of both G91 and G92 steels, and development of creep-fatigue models applicable to advanced ferritic/martensitic alloys. The Cyclic Softening Model and Stress Relaxation Model will be improved by incorporating microstructural parameters of dislocation density, subgrain structure and second-phase particles. Collaborative modeling of combined Cyclic Softening Model, Stress Relaxation Model, and Interactive Damage Rate Model will be pursued for life prediction under creep-fatigue loading with extended hold time. Accelerated, well-controlled creep-fatigue tests will be conducted to provide high-quality experimental data to refine key material parameters and validate and verify models.

## References

Asayama, T., Final Report on Task 10, DOE/ASME NGNP/ Gen IV Materials Project, Oct. 2006.

Asayama, T. and Y. Tachibana, Final Report on Task 5, DOE/ASME NGNP/ Gen IV Materials Project, Sept. 2007.

Asayama, T. et al, ASME Code Week, SGETD meeting, 2010.

ASME NH-Boiler and Pressure Vessel Code, Section III, Division 1, Subsection NH, Class 1 Components in Elevated Temperature Service, American Society of Mechanical Engineers, New York, NY (2011).

Bannantine, A, J. J. Comer and J. L. Handrock, *Fundamentals of Metal Fatigue Analysis*, Prentice-Hall, Inc., 1990.

Blass, J.J. et al., *First Annual Report, Background Review and Study Plan, JAPC-USDOE Joint Study on Structural Design Methods and Data for Modified 9 Cr-1 Mo Steel,* ORNL/9CR/89-1, Oak Ridge National Laboratory, February 1989.

Blass, J.J. et al., Interim Report for the Period April 1- September 30, 1989, JAPC-USDOE Joint Study on Structural Design Methods and Data for Modified 9 Cr-1 Mo Steel, ORNL/9CR/89-3, Oak Ridge National Laboratory, September 1989.

Blass, J.J. et al., Annual Report for the Period April 1,1989 - March 31,1990, JAPC-USDOE Joint Study on Structural Design Methods and Data for Modified 9 Cr-1 Mo Steel, ORNL/9CR/90-2, Oak Ridge National Laboratory, February 1990.

Blass, J.J. et al., Interim Report for the Period April 1-September 30, 1990, JAPC-USDOE Joint Study on Structural Design Methods and Data for Modified 9 Cr-1 Mo Steel, ORNL/9CR/90-3, Oak Ridge National Laboratory, November 1990.

Blass, J.J. et al., Annual Report for the Period April 1,1990 - March 31,1991, JAPC-USDOE Joint Study on Structural Design Methods and Data for Modified 9 Cr-1 Mo Steel, ORNL/9CR/91-1, Oak Ridge National Laboratory, March 1991.

Blass, J.J. et al., JAPC-USDOE Joint Study on Structural Design Methods and Data for Modified 9 Cr-1 Mo Steel, ORNL/9CR/92-2, Oak Ridge National Laboratory, December 1992.

DiStefano, J. R., V. K. Sikka, et al., ORNL-6303, Oak Ridge National Laboratory, Oct. 1986.

Feltham, P. J. Inst. Met. 89 (1961) 219.

Jaske, C. E., B.N. Leis, and C. E. Pugh, 1975, Oak Ridge National Laboratory, CONF-751106-61975.

Kannan, R., R. Sandhya, V. Ganesan, M. Valsan, K. Bhanu Sankara Rao, J. Nucl. Mater. 384 (2009) 286.

Kim, S. and J.R., Weertman, Metall Trans. A 19A (1988) 999.

Li, M., S. Majumdar, and K. Natesan, ANL-GenIV-162, Argonne National Laboratory, 2010.

Li, M., S. Majumdar, W. K. Soppet, D. Rink, and K. Natesan, unpublished information, Argonne National Laboratory, 2011.

Majumdar, S. and P.S. Maiya, Inelastic Behavior of Pressure Vessel and Piping Components, PVP-PB-028, American Society of Mechanical Engineers, New York, 1978, p. 43-54.

Majumdar, S. and P. S. Maiya, Can. Metall. Q, Vol. 18, 1979, p. 57.

Majumdar, S. and P. S. Maiya, J. Eng. Mater. Technol. Vol. 102, 1980, p. 159.

Majumdar, S. and P.S. Maiya, M.K. Booker, unpublished information, Argonne National Laboratory, 1981.

Manson, S.S. and M.H. Hirschberg, *Fatigue: An Interdisplinary Approach*, Syracuse University Press, Syracuse, N.Y., 1964, p.133

Marshall, P. Austenitic Stainless Steels: Microstructure and Mechanical Properties. Elsevier Applied Science Publishers, Ltd. 1984.

Matsuoka, S., S. Kim, and J. R. Weertman, 1984, pp. 507-16 in Proc. Topical Conference on Ferritic Alloy for Use in Nuclear Energy Technologies, Snowbird, Utah, June 19-23, 1983, The Metallurgical Society of the American Institute of Mining, Metallurgical, and Petroleum Engineers, New York.

Natesan, K., Meimei Li, S. Majumdar, R. K. Nanstad, and T. -L. Sham, “Resolution of Qualification Issues for Existing Structural Materials,” ANL-AFCI-285, 2009.

Natesan, K., Meimei Li, S. Majumdar, R. K. Nanstad, and T. -L. Sham, “Code Qualification of Structural Materials for AFCI Advanced Recycling Reactors,” ANL-AFCI-244, 2008.

Riou, B., "Step Forward in Negligible Creep and Creep-Fatigue of Mod 9Cr-Mo" ASME Subgroup on Elevated Temperature Design submittal, Attachment #6 to November, 2007 ASME B&PV Code, SG-ETD Meeting Minutes (2007).

Shankar, V., M. Valsan, K. Bhanu Sankara Rao, R. Kannan, S. L. Mannan, S. D. Pathak, Mater. Sci. Eng. A 437 (2006) 413.

**Nuclear Engineering Division**
Argonne National Laboratory
9700 South Case Avenue
Argonne, IL 60439

www.anl.gov

Argonne National Laboratory is a U.S. Department of Energy
laboratory managed by UChicago Argonne, LLC